



**Politecnico
di Torino**

Politecnico di Torino
Biomedical Engineering
A.a. 2023/2024
Sessione di Laurea Ottobre 2024

Coma Outcome Predictive Analysis

Identification of suitable indicators with a main focus on
brain connectivity

Relatori:
Mesin Luca

Candidati:
Agresti Matteo

Contents

| | | |
|----------|---|-----------|
| 1 | Introduction | 3 |
| 1.1 | The central nervous system | 3 |
| 1.1.1 | General introduction to the central nervous system | 3 |
| 1.1.2 | The neurons | 7 |
| 1.1.3 | The glial cells | 9 |
| 1.1.4 | The brain | 11 |
| 1.2 | The electroencephalogram | 14 |
| 1.2.1 | History of the EEG | 14 |
| 1.2.2 | Introduction to EEG | 15 |
| 1.2.3 | EEG Recording System | 19 |
| 1.3 | Cognitive Function and Consciousness | 21 |
| 1.3.1 | Understanding Consciousness | 21 |
| 1.3.2 | Disorders of Consciousness | 23 |
| 1.3.3 | Brain Death | 25 |
| 2 | State of art | 28 |
| 2.1 | Why this field of study?..... | 28 |
| 2.2 | Scales to evaluate awarness [20]..... | 29 |
| 2.3 | Data acquisition tempistics | 30 |
| 2.4 | Outcome prediction methodologies | 31 |
| 2.5 | Examples of studies on prediction based on various methods..... | 32 |
| 2.5.1 | First Example [22]..... | 32 |
| 2.5.2 | Second Example [34]..... | 33 |
| 2.5.3 | Third Example [18] | 34 |
| 2.5.4 | Fourth Example [28]..... | 35 |
| 2.5.5 | Fifth Example [10] | 36 |
| 2.5.6 | Sixth Example [32]..... | 37 |
| 2.5.7 | Seventh Example [36] | 39 |

| | |
|---|-----------|
| 3 Methods | 41 |
| 3.1 Dataset | 41 |
| 3.2 Preprocessing | 41 |
| 3.3 Indicators Extraction | 42 |
| 3.4 Statistical Metrics | 48 |
| 3.5 Features Selection..... | 49 |
| 3.6 Classification | 50 |
| 3.6.1 Fisher's Linear Discriminant (FLD)..... | 50 |
| 3.6.2 Support Vector Machine (SVM)..... | 51 |
| 3.6.3 Decision Tree | 52 |
| 3.6.4 K-Nearest Neighbors (K-NN) | 53 |
| 3.7 Methods of Evaluation | 54 |
| 3.8 Cross-Validation | 57 |
| 4 Results | 58 |
| 4.1 Results of the NSF-based method | 58 |
| 4.1.1 NSF-B - Fisher | 60 |
| 4.1.2 NSF-B - Support Vector Machine | 61 |
| 4.1.3 NSF-B - Decision Tree..... | 62 |
| 4.1.4 NSF-B - k-Nearest Neighbors | 63 |
| 4.2 Results of the SF-based one-size method | 64 |
| 4.2.1 SF-B-OS - Fisher | 65 |
| 4.2.2 SF-B-OS - Support Vector Machine | 66 |
| 4.2.3 SF-B-OS - Decision Tree | 67 |
| 4.2.4 SF-B-OS - k Nearest Neighbors..... | 68 |
| 4.3 Results of the SF-based tailored method..... | 69 |
| 4.3.1 SF-B-T - Fisher | 70 |
| 4.3.2 SF-B-T - Support Vector Machine..... | 71 |
| 4.3.3 SF-B-T - Decision Tree | 72 |
| 4.3.4 SF-B-T - k Nearest Neighbors | 73 |
| 4.4 Considerations..... | 74 |
| 5 Conclusion | 75 |

Chapter 1

Introduction

This chapter will explain: the central nervous system, the electroencephalogram (EEG), and the current understanding of consciousness along with its associated disorders.

1.1 The central nervous system

The contents of this section are based on [19].

1.1.1 General introduction to the central nervous system

The Central Nervous System (CNS) represents a complex framework with seven main components: the spinal cord, medulla oblongata, pons, cerebellum, midbrain, diencephalon, and cerebrum. The spinal cord is the lowest part of the CNS and can be split into four regions: cervical, thoracic, lumbar, and sacral (Figure 1). It handles sensory information coming from the skin, joints, and muscles in the limbs and trunk, and it controls the movements of these areas.

As we progress rostrally, the spinal cord transitions into the brain stem, which encompasses the medulla oblongata, pons, and midbrain. It is of crucial importance in:

- processing sensory data from the skin and muscles of the head;
- controlling the motor functions of head musculature;

- facilitating the transmission of information between the spinal cord and the higher brain regions;
- regulating arousal and consciousness through its involvement with the reticular formation.

The brain stem is home to various clusters of cell bodies, known as cranial nerve nuclei. These nuclei serve various functions:

- receiving input from the skin and muscles of the head;
- controlling motor functions of the face, neck, and eyes;
- processing information from three distinct senses: hearing, balance, and taste.

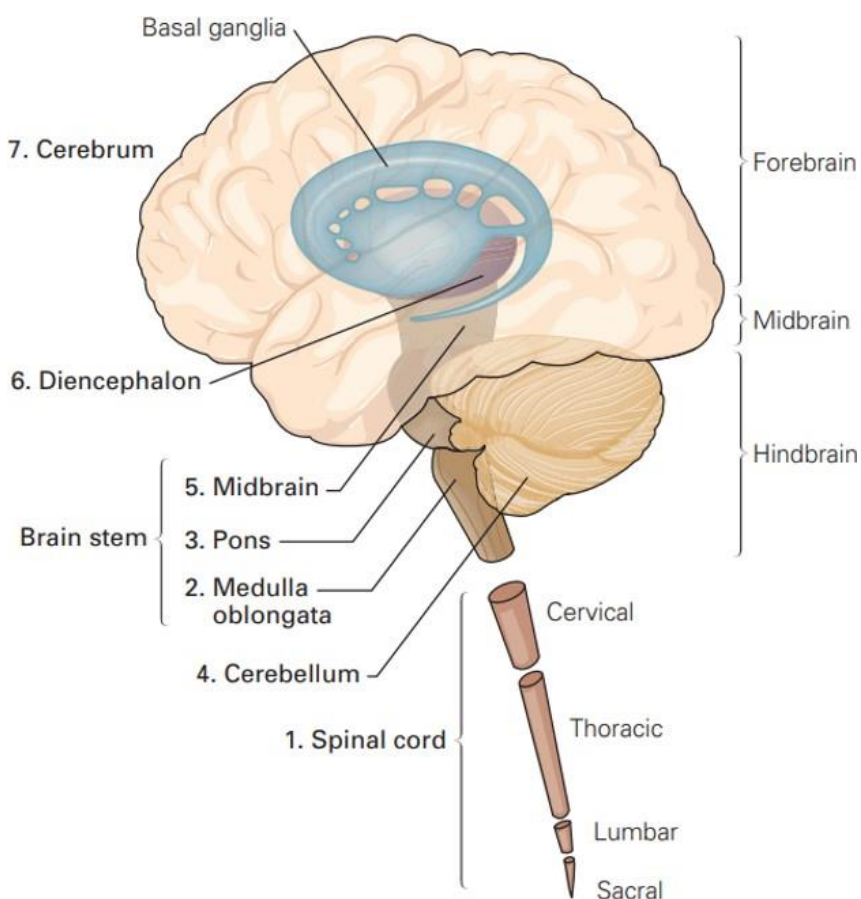


Figure 1.1: Division in seven parts of the central nervous system [19]

Directly rostral to the spinal cord, the medulla oblongata boasts several centers responsible for overseeing critical autonomic functions like digestion, respiration, and heart rate regulation, while, situated in front of the medulla, the pons acts as a bridge for conveying motor signals from the cerebral hemispheres to the cerebellum.

The cerebellum, located behind the pons, forms connections with the brain stem via major fiber tracts known as peduncles. This region is instrumental in modulating the force and range of movement and plays a pivotal role in learning and executing motor skills.

Moving further rostrally, the midbrain, found anterior to the pons, governs a wide array of sensory and motor functions, including eye movement and the coordination of visual and auditory reflexes.

The diencephalon, situated rostral to the midbrain, encompasses two distinct structures: the thalamus and the hypothalamus. The thalamus is the hub for most of the sensory information relayed to the cerebral cortex from various parts of the central nervous system, while the hypothalamus assumes responsibility for regulating autonomic, endocrine, and visceral functions.

The cerebrum consists of two cerebral hemispheres, each of whom comprises a highly convoluted outer layer known as the cerebral cortex, along with three deeper structures: the basal ganglia, the hippocampus, and the amygdaloid nuclei. The cerebral cortex is further partitioned into four separate lobes: frontal, parietal, occipital, and temporal, as elucidated in Figure 2.

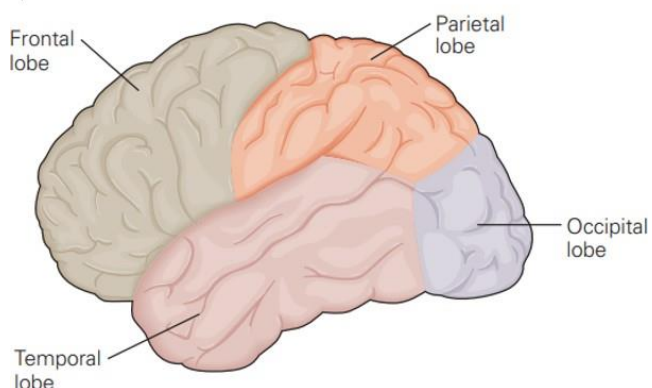


Figure 1.2: The four lobes of the cerebral cortex [19]

Within this context, the basal ganglia play a pivotal role in governing motor performance, the hippocampus is closely associated with certain aspects of memory storage, and the amygdaloid nuclei coordinate autonomic and endocrine responses during emotional states.

The brain can be broadly divided into three main regions: the hindbrain (comprising the medulla oblongata, pons, and cerebellum), the midbrain, and the forebrain (comprising the diencephalon and cerebrum).

The cells that primarily compose the CNS can be categorized into two groups: neurons and glial cells.

1.1.2 The neurons

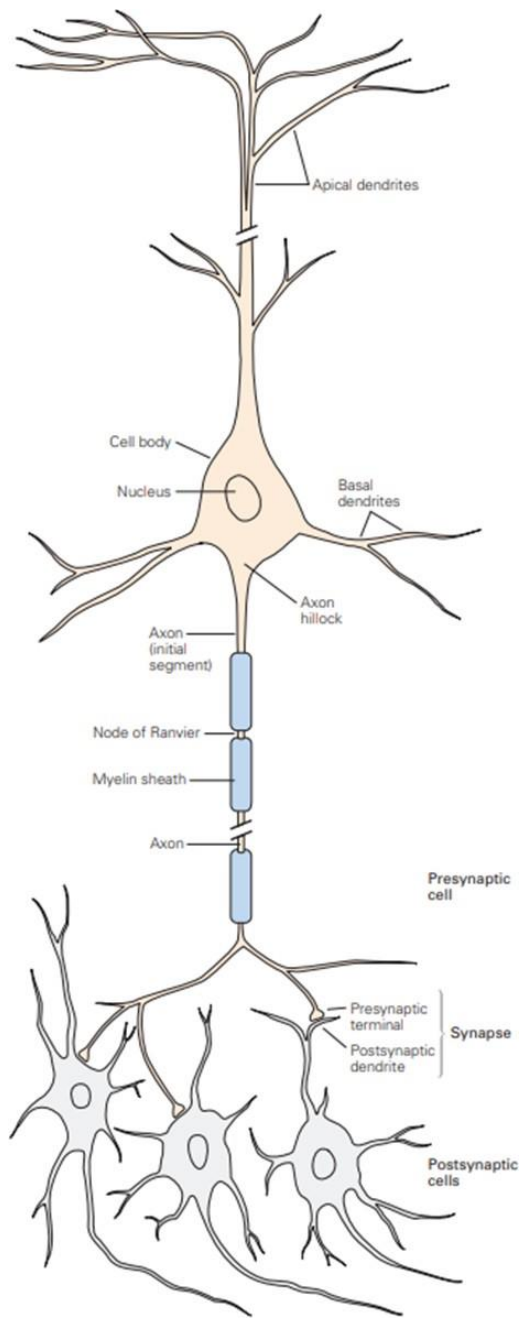


Figure 1.3: The structure of a neuron [19]

Neurons, commonly referred to as nerve cells, form the basic units of the CNS, with the human brain containing around one hundred billion neurons classified into at several different types.

Neurons share a standard structural framework, encompassing four distinct regions: cell body, dendrites, axon, and presynaptic terminals, as depicted in Figure 3. Each of these regions plays a unique role in signal generation and the facilitation of communication between neurons.

The cell body, or soma, serves as the neuron's metabolic center, housing the nucleus with the cell's genetic material and the endoplasmic reticulum that synthesizes proteins, typically giving rise to multiple short dendrites and a single axon of significant length.

Dendrites structurally resemble the branches of a tree and serve as the primary apparatus for receiving incoming signals from neighboring neurons, while the axon extends a considerable distance from the cell body, acting as a conduit for transmitting signals to other neurons. An axon can convey electrical signals across distances spanning from 0.1 millimeters to 2 meters.

These electrical signals, referred to as action potentials, originate at a specialized trigger region near the axon's origin, known as the initial segment. These impulses propagate down the axon with remarkable consistency and speed, regenerating at regular intervals along it, covering distances ranging from 1 to 100 meters per second, and traveling through the axon at a near-constant amplitude of 100 millivolts, owing to its all-or-nothing nature.

Action potentials serve as the fundamental signals that enable the brain to receive, process, and transmit information. These signals maintain a highly stereotyped nature throughout the nervous system, regardless of the diverse array of environmental stimuli that trigger them, such as light, mechanical contact, odorants, and pressure waves. The brain, in turn, interprets patterns of incoming electrical signals and their pathways, ultimately giving rise to our sensory experiences of sight, touch, smell, and sound.

To enhance the conduction speed of action potentials, larger axons are enveloped in an insulating sheath composed of a lipid substance called myelin, and that is periodically interrupted by uninsulated regions known as nodes of Ranvier, where the action potential undergoes regeneration. As the axon approaches its terminus, it divides into fine branches that establish connections with other neurons at spe-

cialized communication points referred to as synapses.

Amongst the neurons, the one transmitting a signal assumes the role of the presynaptic cell, while the recipient one that of the postsynaptic cell. Signals are transmitted by the presynaptic cell from distinct, enlarged regions at the ends of its axonal branches, denoted as presynaptic terminals or nerve terminals. These two cells are separated by a narrow gap known as the synaptic cleft, and while most presynaptic terminals end on the dendrites of the postsynaptic neuron, they may also terminate on the cell body or, less commonly, at the beginning or end of the axon of the receiving cell (refer to Figure 3).

Sensory neurons, motor neurons, and interneurons are the three primary groups into whom the nerve cells may be classified.

Sensory neurons, often referred to as afferent neurons, transmit information, important for both perception and motor coordination, from the peripheral sensors of the body to the nervous system. It is worth noting that the term "sensory" should be specifically applied to afferent inputs leading to perception, while the term "afferent" encompasses all data originating from the periphery, regardless of its relation to sensation.

Motor neurons (aka efferent neurons) transmit commands from the brain or spinal cord to muscles and glands, carrying efferent information. Interneurons can be categorized into relay and local interneurons. The former have long axons and send signals over long distances, linking different brain regions, whereas the latter have shorter axons and connect with nearby neurons within local circuits.

Furthermore, each of these primary functional classifications can be subdivided further. In the case of sensory system interneurons, their categorization can be based on the type of sensory stimuli they respond to, and these initial classifications can be further refined based on factors like location, density, and size.

1.1.3 The glial cells

Glial cells vastly outnumber the neurons within the vertebrate central nervous system, with estimates suggesting there are 2 to 10 times more glial cells than neurons. Although historically named after the Greek word for "glue," these cells do not primarily serve as binding agents for nerve cells, instead, they envelop the cell bodies, axons, and dendrites of neurons, playing crucial supporting roles. Glial cells differ in both form and function from neurons, as they lack dendrites

and axons and do not share the same membrane properties, rendering them non-electrically excitable and not directly involved in electrical signaling, the primary domain of nerve cells.

The vertebrate nervous system contains various types of glial cells that exhibit significant diversity in morphology, similar to the diversity observed in neurons, and because of this, they can generally be divided into two main categories: microglia and macroglia. Microglia act as immune system cells, becoming active in response to injuries, infections, or degenerative diseases, and are involved in antigen presentation and phagocytosis.

Macroglia, which constitute around 80% of all cells in the human brain, encompass three primary types: oligodendrocytes, Schwann cells, and astrocytes. Oligodendrocytes and Schwann cells, both relatively small with few processes, play a key role in insulating axons by wrapping their membranous processes around axons in a spiral, forming the myelin sheath. Oligodendrocytes are located in the central nervous system and envelop one to 30 axonal segments (known as internodes) depending on axon diameter, whereas Schwann cells are found in the peripheral nervous system and envelop a single segment of one axon. Myelinating axons by both oligodendrocytes and Schwann cells enhance signal conduction and organize voltage-sensitive ion channels within distinct axonal regions known as nodes of Ranvier.

Astrocytes, the third major type of glial cells, are named for their irregular, star-shaped cell bodies and numerous processes; there are two main types of astrocytes, protoplasmic and fibrous, with protoplasmic astrocytes predominantly found in the gray matter, each serving distinct roles. They have processes that end in sheet-like appendages, enveloping nerve cell bodies and synapses. In contrast, fibrous astrocytes are typically located in the white matter, possessing fine, elongated processes containing tightly packed intermediate filaments.

Both types of astrocytes exhibit end-feet that make contact with and surround capillaries and arterioles throughout the brain. Protoplasmic astrocytes play a crucial role in enveloping nerve cell bodies and synapses with their sheet-like processes, while the end-feet of fibrous astrocytes contact axons at the nodes of Ranvier.

The precise functions of astrocytes remain enigmatic, but there are several established roles:

- Separate cells, insulating neuronal groups, and synaptic connections.
- Regulate K⁺ concentration in the extracellular space between neurons.

- Uptake excess K⁺ to maintain efficient signaling between neurons.
- Perform housekeeping tasks, including the uptake of neurotransmitters from synaptic zones after release.
- Support neighboring neurons by releasing growth factors.

1.1.4 The brain

The central nervous system exhibits bilateral symmetry and consists of two principal components: the spinal cord and the brain, with the brain being a remarkably intricate organ that houses seven major regions, as depicted in Figures 1 and 4. Modern advancements in radiographic imaging techniques have allowed for the observation of these structures in real-time within living individuals, a significant breakthrough that has revolutionized our understanding of the brain.

These innovative brain imaging techniques have become invaluable tools for assessing the metabolic activity of specific brain regions during the execution of specific tasks under controlled conditions, furnishing direct evidence regarding the connection between various types of behavior and specific brain regions.

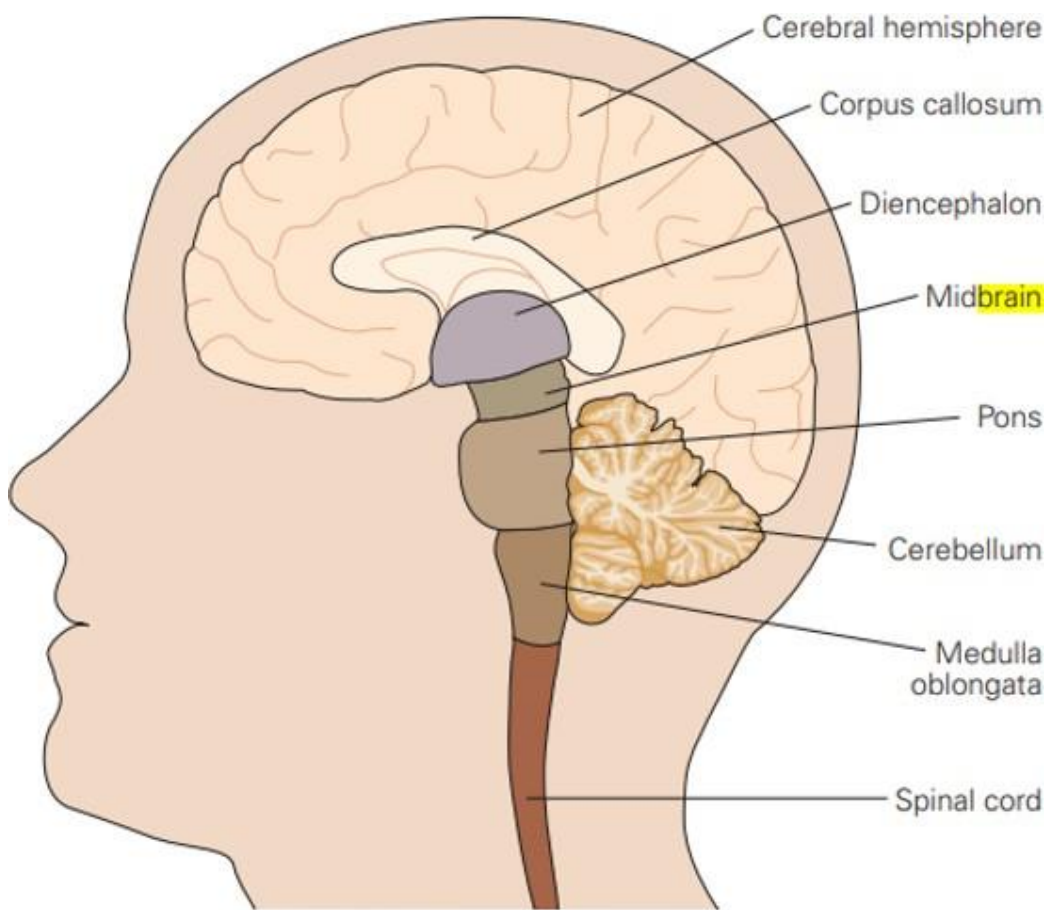


Figure 1.4: Position of major structures of the brain in relation to external landmarks [19]

Researchers taking a cellular connectionist approach to the study of the brain have made significant strides in pinpointing the neural processes underpinning our cognitive abilities. These processes are predominantly located in the cerebral cortex, the highly convoluted gray matter enveloping the two cerebral hemispheres. Each hemisphere's cortical surface is divided into frontal, parietal, occipital, and temporal lobes, named after the cranial bones covering them, as depicted in Figure 2.

The characteristic deep folds on the cortex, known as gyri, and the recesses between them, referred to as sulci or fissures, are evolutionary adaptations to accommodate a greater number of nerve cells within a confined space. Several prominent gyri and sulci bear specific names, such as the central sulcus, which demarcates the precentral gyrus, responsible for motor function, from the postcentral gyrus, dedicated to sensory functions, as depicted in Figure 5. Each lobe of the cerebral

cortex has its own specific functions:

- The frontal lobe is mainly involved in short-term memory, planning future actions, and controlling motor functions.
- The parietal lobe plays a key role in somatic sensation, body image formation, and its relation to the external world.
- The occipital lobe is in charge of handling visual information.
- The temporal lobe, including its deep structures such as the hippocampus and amygdaloid nuclei, plays a role in hearing, learning, memory, and emotional processing.

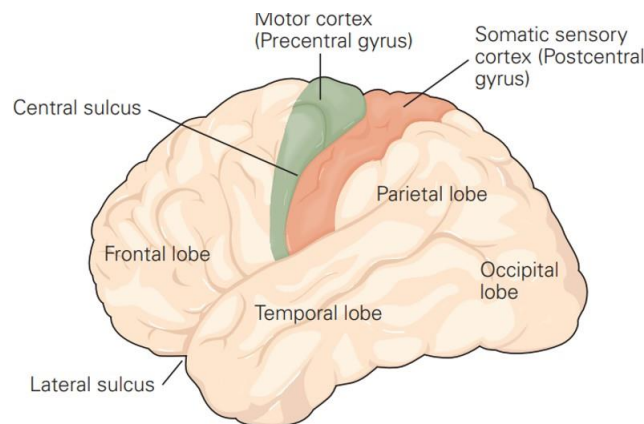


Figure 1.5: The four lobes of the cerebral cortex [19]

The cerebral cortex is organized in two hemispheres that are apparently similar, but not completely symmetrical in structure or function. Each of those primarily manages sensory and motor functions for the opposite side of the body, making it so that sensory input from the left side of the body crosses to the right side of the nervous system before reaching the cerebral cortex, while the motor regions in the right hemisphere govern movements on the left side of the body.

1.2 The electroencephalogram

The contents of this section are based on [6], [33] and [2].

1.2.1 History of the EEG

The history of epilepsy is extremely ancient, encompassing various cultures such as Mesopotamia, Akkadian, and ancient Babylonians around 2000 BCE (Before Common Era), as well as the Greeks in the 5th to 4th century BCE. Over the centuries, an array of therapeutic approaches emerged to address epilepsy, categorizing them into four primary methods: conventional, peripheral, trepanation, and religious procedures.

The modern era of electroencephalography (EEG) has its origins in medieval times, with early pioneers like Gilbert, Galileo, and Willis exploring the electrical properties of various substances. In 1672, Otto von Guericke developed the first electrostatic apparatus capable of generating static electricity. However, EEG as a distinct field truly began in 1875 when Richard Caton recorded electrical impulses from the brains of monkeys and rabbits using a galvanometer, marking the start of electrical brain activity recordings. It further advanced in 1890 thanks to Ernst von Fleischl-Marxow, who demonstrated an important connection between nervous system activity and muscle movements.

Concurrently, Beck's investigations in the same era identified consistent electrical activity in the brains of dogs and rabbits. The groundwork laid by Hermann von Helmholtz, a German physician and physicist, for the precise measurement of nerve conduction velocity is noteworthy.

In 1901, Dutch physiologist Wilhelm Einthoven introduced the first string galvanometer, a pivotal milestone in modern electrocardiography. Subsequently, the development of various forms of galvanometers followed, including Gustav Wiedemann's six-coil galvanometer and the Helmholtz tangent galvanometer. The year 1910 witnessed Berger's pioneering utilization of a string galvanometer for EEG recordings, further propelling the field's advancement.

From this juncture, the field of EEG rapidly progressed and began to be applied extensively in clinical and experimental epilepsy studies as well as broader neurological research.

1.2.2 Introduction to EEG

The Electroencephalogram (EEG) is a crucial technique used to record the electrical activity generated by the human brain. Its remarkable sensitivity to temporal changes makes it an essential tool for assessing the dynamic functioning of the brain. In the realm of clinical diagnosis, EEG plays a pivotal role, especially in the identification of patients with suspected seizures, epilepsy, or unusual neurological episodes. In epilepsy, their recordings typically show characteristic changes during seizures and often include interictal epileptiform discharges (IEDs), such as spikes (lasting < 70 μ sec), spike-and-wave patterns, or sharp-wave discharges (lasting 70–200 μ sec) between seizures.

Beyond epilepsy, EEG finds applications across a spectrum of clinical scenarios. An example is the role that it plays in monitoring the depth of anesthesia during surgical procedures. Its sensitivity to rapid changes in neural activity proves instrumental in the early detection of potential complications such as ischemia or infarction. In both clinical and research settings, EEG waveforms can be averaged, yielding evoked potentials (EPs) and event-related potentials (ERPs), thereby enabling the analysis of neural activity in response to specific stimuli.

EEG signals are primarily believed to originate from the cortical pyramidal neurons situated in the cerebral cortex. These neurons are oriented perpendicular to the brain's surface, and the EEG records the summation of postsynaptic potentials, both excitatory and inhibitory, emanating from synchronized neuronal groups.

However, it's essential to note that traditional scalp or cortical surface EEG recordings cannot capture the transient local field potential changes resulting from neuronal action potentials. Furthermore, electrical activity from extracranial sources or the environment can often obscure cerebral activity in EEG recordings. Thus, the data acquired in EEG must pass through several biological and anatomical filters as they traverse the brain, cerebrospinal fluid (CSF), meninges, skull, and skin before they can be detected at the recording site. It is important to note that electrical activities from scalp muscles, eyes, tongue, and even the heart can generate substantial voltage potentials, which can sometimes overshadow and obscure cerebral activity, and temporary disruptions of the recording electrodes, known as "electrode pop" artifacts, can degrade EEG quality or even mimic brain rhythms and seizures. These electrical artifacts present a common challenge in EEG interpretation but can be recognized by software or experienced observers thanks to the distinctive features that many of them have.

In its standard format, EEG is presented with voltage on the ordinate axis and time on the abscissa axis, providing a nearly real-time representation of ongoing brain activity (see Figure 6). During the digital recording and review process, adjustments to various aspects of the EEG display can be made for better data visualization and clarity. These adjustments include altering the sensitivity, also known as "gain," which is generally measured in microvolts per millimeter, to modify the amplitude of the waveforms. The time scale displayed, even referred to as "paper speed," can be adjusted to either shorter intervals for the rapid identification of brief EEG events such as epileptiform spikes or longer intervals for analyzing slowly evolving rhythmic discharges. The application of digital filters to reduce artifacts is to be approached with caution, as these filters may inadvertently distort EEG waveforms of interest.

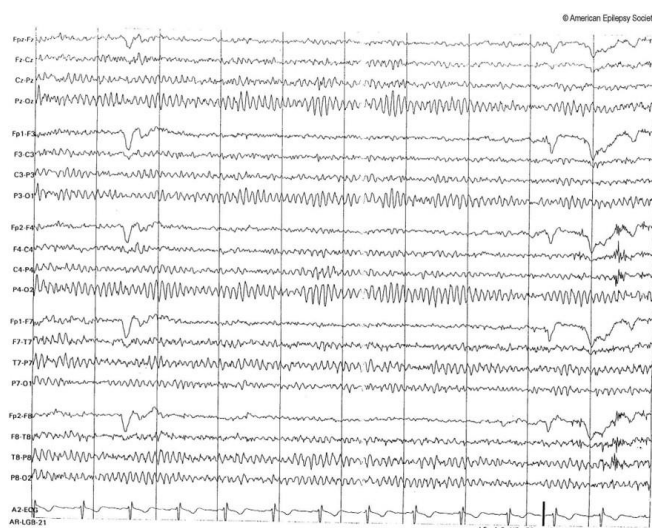


Figure 1.6: Normal EEG with typical montage. [6]

EEG functions based on the principle of differential amplification. It measures voltage differences between different electrode points, allowing distinguishable EEG waveforms to be generated. Conventionally, when the active exploring electrode (referred to as G1, or "Grid 1") is more negative than the reference electrode (G2), the EEG potential vector points upward above the horizontal meridian, resulting in an upward wave. Conversely, when the reference electrode has a more negative charge, the EEG potential vector shifts downward, falling below the horizontal meridian. Figure 7 illustrates other polarity possibilities.

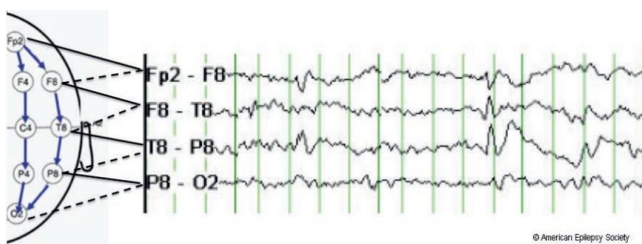


Figure 1.7: Polarity conventions and localization in EEG. [6]

A systematic approach to EEG analysis entails consideration of five key components: calibration, orientation and nomenclature, montages, frequency bands, and clinical context.

Before interpreting the EEG, it is essential to ensure proper calibration of the study by introducing a known voltage into the system to verify uniform amplification across all channels, as any irregularities in amplification at this stage could significantly affect subsequent EEG interpretation. To further confirm the accuracy of the cerebral signal, biocalibration is performed, which usually involves having the patient open and close their eyes.

Understanding EEG nomenclature is paramount before commencing interpretation. In 1958, the International Federation for Electroencephalography and Clinical Neurophysiology introduced a standardized electrode placement system known as the 10-20 electrode positioning system (Refer to Figure 11 for the standard International 10-20 electrode site placement strategy). This system established a consistent method for the physical placement and identification of electrodes on the scalp. The cranium is divided into proportional segments based on key skull landmarks (nasion, preauricular points, inion) to ensure comprehensive coverage of all cerebral regions. The 10-20 system refers to the percentage-based distances between the ears and the nose, which are used to determine the placement of electrode positions.

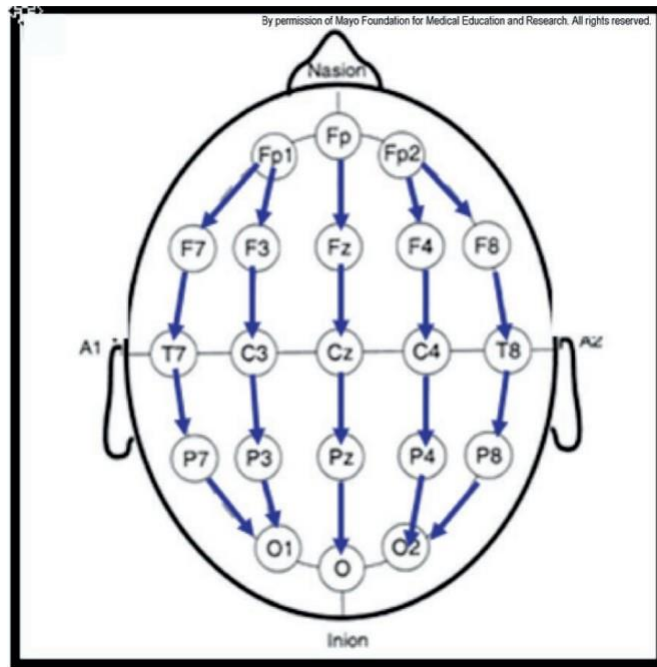


Figure 1.8: The International 10-20 electrode placements. [6]

Electrode positions are identified based on adjacent cerebral areas: F for frontal, C for central, T for temporal, P for posterior, and O for occipital regions. These letters are accompanied by odd numbers on the left side of the head and even numbers on the right side, with left and right defined conventionally from the subject's perspective, "z" denotes midline locations from front to back, and "A" designates auricular sites on the mastoid processes. Each electrode is situated in proximity to specific cerebral centers, reflecting various cognitive functions. For example, F7 is positioned near regions responsible for rational thought, Fz is close to intentional and motivational centers, and F8 is in proximity to sources of emotional impulses. The cortex surrounding locations C3, C4, and Cz is involved in sensory and motor functions. P3, P4, and Pz areas contribute to perceptual and differentiation activities, while emotional processing centers are found near T3 and T4. Certain memory functions are associated with T5 and T6, and the primary visual areas are situated beneath points O1 and O2.

Calibration verification is essential to ensure uniform amplification across all channels.

1.2.3 EEG Recording System

The EEG recording system encompasses several components that work together to capture, process, and interpret electrical brain activity. They include electrodes equipped with conductive material, amplifiers with filters, an A/D converter, and a recording device.

Electrodes come in various types, each with distinct characteristics. The main electrode categories encompass disposable (gel-less and pre-gelled), reusable disc electrodes (gold, silver, stainless steel, or tin), headbands, electrode caps, saline-based electrodes, and needle electrodes. Each type serves particular purposes and necessitates specific skin preparation and conductive mediums to ensure optimal contact.

Amplifiers are designed to selectively amplify the physiological signal, filter out unwanted noise and interference, and safeguard both patients and electronic equipment from voltage and current surges. Crucial requirements for a biopotential amplifier include not influencing the monitored physiological process, avoiding distortion of the measured signal, maximizing the separation of signal and interference, protecting the patient from electric shock hazards, and safeguarding the amplifier from damage caused by high input voltages, such as those occurring during defibrillation or electrosurgery.

The input signal to the amplifier encompasses five components: the desired biopotential, undesired biopotentials, power line interference (50/60 Hz and its harmonics), interference signals from the tissue/electrode interface, and noise. Well-designed amplifiers can reject a substantial portion of these signal interferences. The desired biopotential is manifested as a differential signal between the two input terminals of the differential amplifier. The amplifier's gain represents the ratio of the output signal to the input signal, and this gain should be chosen to ensure optimal signal quality and an adequate voltage level for further processing.

For clinical applications, a shielded room to minimize urban electrical background noise is generally not required, but it may be employed for research purposes seeking maximal information. In such research cases, amplifiers powered by batteries and an optical cable connecting to a PC located outside the shielded area are typically used. Electrical/optical and optical/electrical converters are also required in such setups. To eliminate line noise, low-pass filters with a cutoff below 50/60 Hz are commonly used.

When digital recording devices are employed, analog signals from each channel are

repeatedly sampled at fixed time intervals (sampling interval), and converted into digital data by an A/D converter. The converter is then connected to a computer system, where each sample is stored in memory. The resolution of the A/D converter is determined by dividing the converter's voltage range by 2 raised to the power of the number of bits, with a minimum of 12 bits typically used (providing 4,096 value levels). It should have the ability to resolve 0.5 μ V. It is required for the sampling rate to be at least twice the highest frequency component of interest. Analog filters are incorporated into the amplification unit to reduce low frequencies originating from bioelectric potentials. A high-pass filter with a cutoff frequency typically between 0.1-0.7 Hz is used to eliminate these low frequencies and ensure the signal is band-limited. This is critical to prevent signal distortion due to aliasing, which can occur if frequencies above the Nyquist limit are not excluded before digitization.

The choice of a digital recording device is contingent on the intended purpose of the EEG study. Digital systems provide the flexibility to display EEG waveforms simultaneously in various time bases, from 30 s/page to 2 mm/s, facilitating an accurate interpretation of events, such as ictal behaviors. In most digital EEG systems, the continuous analog signal is directly filtered before digitization to prevent aliasing and stored as a digitized signal. The advantages of digital EEG recording encompass the ability to readily review raw EEG data, apply digital filters, perform spectral analysis, and utilize quantitative EEG (qEEG) techniques. The use of digital systems also allows further storage and data compression, enabling easier long-term storage and retrieval.

1.3 Cognitive Function and Consciousness

The contents of this section are based on [19], [1], [14], [24] and [29].

1.3.1 Understanding Consciousness

To gain insights into the biological processes governing cognition, it is imperative to transcend individual neurons and delve into the intricacies of information processing within neural networks. This endeavor mandates not only the application of techniques and methodologies from cellular and systems neuroscience but also the incorporation of cognitive psychology insights.

The anterior section of the parietal lobe creates important mental maps of the body's surface and the space around it based on our experiences. The examination of alterations within the posterior parietal association cortex demonstrates the pivotal role of selective attention in integrating internal body representation with the perception of external spatial surroundings. This integration extends to encompass the representation of the body concerning real, imagined, or remembered visual space, with self-awareness embedded within this unified representation. Russian neuropsychologist A. R. Luria suggested that portions of the parietal lobe constitute the most distinctly human aspect of cortical organization.

It is crucial to acknowledge that multiple forms of consciousness exist, each characterized by distinctive neural representations. For instance, Edelman and Damasio differentiate between primary (core) consciousness and higher-order (extended) consciousness. Primary consciousness entails an awareness of objects in the world and the capacity to generate mental images. This form of consciousness is not exclusive to humans but is also shared by nonhuman primates and potentially other vertebrate animals. In contrast, higher-order consciousness encompasses an awareness of being conscious, representing a uniquely human trait. This form of consciousness facilitates the conceptualization of past and future events, enabling individuals to contemplate the consequences of their actions and emotions.

In their pursuit of a comprehensive reductionist approach to the study of consciousness, Crick and Koch built upon Sigmund Freud's perspective, which posits that a significant portion of mental functions remains unconscious, including a substantial portion of thinking. Our consciousness primarily concerns the sensory representations of mental activities.

Conventionally, consciousness is construed as a state of self-awareness. Eminent philosophers of the mind, such as John Searle and Thomas Nagel, have outlined three fundamental aspects of self-awareness: subjectivity, unity, and intentionality.

Subjectivity, within the context of self-awareness, presents a significant philosophical and scientific challenge. It suggests that every individual possesses an awareness of self that serves as the epicenter of their experiences. Our experiences, encompassing thoughts, moods, sensations, triumphs, disappointments, joys, and pains, are directly lived and carry a profound sense of reality, eclipsing the experiences of others. The fundamental subjectivity of conscious experience raises questions regarding the possibility of objectively discerning characteristics of consciousness that transcend individual experience.

The unity of self-awareness refers to the idea that, at any given moment, our perception forms a single, coherent experience in which all sensory inputs merge into one unified perception.

Self-awareness exhibits intentionality, signifying that conscious experience links successive moments with a sense of directed purpose. In the past, these attributes of consciousness led some philosophers to embrace dualism, positing that the body and the mind are distinct substances, with the body being physical and the mind existing in a nonphysical, spiritual realm. However, most contemporary philosophers of mind concur that consciousness emerges from the physical properties of the brain.

The discourse on consciousness is characterized by two predominant camps. The first, represented prominently by Daniel Dennett, asserts that consciousness is an outcome of the computational activity in the brain's association areas, rather than being a discrete brain operation. The second camp, encompassing thinkers like Francis Crick, Christof Koch, John Searle, Thomas Nagel, Antonio Damasio, and Gerald Edelman, contends that consciousness constitutes a distinct phenomenon. For a complete understanding of how our experiences are constructed, addressing the issues of subjectivity, unity, and intentionality is paramount.

Consciousness exhibits unique properties not found in other mental functions, rendering a biological explanation a profoundly challenging endeavor. Philosopher Colin McGinn goes so far as to argue that consciousness remains beyond empirical study due to inherent limitations in human intelligence, comparing it to how monkeys cannot comprehend quantum theory. Conversely, Searle and Nagel maintain that consciousness is analyzable, but its complexity and subjectivity impede our

ability to explain it. It stands apart from any other brain function and eludes current scientific inquiry methods.

Among the three facets of consciousness, subjectivity proves the most empirically challenging to dissect. As of now, we lack a comprehensive understanding of how the firing of specific neurons leads to conscious perception. According to Searle, we even lack an adequate theoretical model explaining how objectively observable phenomena in someone else's brain can produce a subjectively experienced sensation, such as pain. Given its inherently subjective nature, consciousness remains elusive to contemporary scientific practices.

Nagel contends that the reductionist approach of current science cannot tackle consciousness without a substantial change in methodology, one that incorporates defining the elements of subjective experience. These elements are likely to be fundamental constituents of brain function, akin to atoms and molecules in the realm of matter. Nagel suggests that reductions from one object to another aren't problematic since we can theoretically comprehend how the properties of a particular type of matter arise from its constituent molecules. What we lack are rules for extrapolating subjective experiences from the physicochemical properties of interconnected nerve cells.

Nagel argues that our limited insight into the elements of subjective experience should not hinder our quest to establish rules that connect conscious phenomena to cellular processes in the brain. He posits that the necessary knowledge for a more fundamental form of analytical reduction, transitioning from something subjective (experience) to something objective (the physical), can only be acquired through accumulating cell-biological data. According to Nagel, only after we've formulated a theory of the mind that supports this novel and profound reduction will we fully comprehend the constraints of current reductionism. Discovering the elementary components of subjective consciousness, according to Nagel, may necessitate a biological revolution and likely a complete transformation of scientific thought.

1.3.2 Disorders of Consciousness

Consciousness, at its core, represents the awareness of self and the surrounding environment. To exhibit conscious behavior, individuals must maintain adequate wakefulness and cognitive awareness of sensory, cognitive, and emotional experiences.

Severe acquired brain injuries (ABIs) result from catastrophic events that disrupt the brain's mechanisms controlling wakefulness (brainstem) and awareness (cortex). The most severe cases lead to persistent disorders of consciousness (DoC), including the vegetative state (VS) and the minimally conscious state (MCS). The vegetative state is also known as post-coma unawareness or unresponsive wakefulness syndrome (UWS). (Table 1)

| DoC | Definition |
|---|---|
| Coma | A state of being completely unconscious. The person is not awake, and the eyes remain constantly closed. Also, there is no behavior suggesting the person is aware of self or surroundings. |
| Vegetative State, or VS Unresponsive Wakefulness Syndrome, or UWS Post-coma Unawareness, or PC-U | A state of being awake, with eyes open, and of not showing signs of behavior suggesting the person is aware of self or surroundings. |
| Persistent Vegetative State, or PVS | A VS or UWS that lasts for more than a month. |
| Minimally Conscious State, or MCS | A state in which the person has definite signs of behavior showing awareness of self or surroundings. Often, these behaviors may not be obvious or may not happen regularly. |
| Emergence from MCS, or EMCS | A state where the person can communicate in a way that can be understood. Or the person can recognize and use familiar objects. <ul style="list-style-type: none"> • To show communication, the person can answer yes or no to questions. The answers may be said aloud, written down, or shown with movements. Examples of these movements are head nodding or shaking, or thumbs pointing up or down. The answers must be correct and consistent when repeated. • For object use, the person can show that he or she knows how to use at least two different everyday objects, such as a cup or a comb. |
| Recovery of Consciousness | A change in behavior that clearly shows the person is recovering awareness of self or surroundings. Recovery of consciousness happens when the health status of someone in a coma or VS/UWS improves to MCS. |

Figure 1.9: Terms Related to DoC [1]

Accurate diagnosis of DoC is crucial, especially during the early stages of recovery post-injury, to ensure appropriate care. Individuals experiencing DoC for 28 days or more require specialized, ongoing healthcare, as outcomes vary significantly. Some individuals remain permanently unconscious, many require assistance with daily tasks due to severe disability, some regain independence to varying degrees, and a few may even return to work.

DoC can result from severe brain injury, which can be categorized as traumatic or non-traumatic:

Traumatic brain injury (TBI) results from physical impacts, such as falls, car accidents, and head injuries sustained during sports.

Non-traumatic brain injury occurs when medical conditions affect critical bodily systems, potentially limiting oxygen supply to the brain. Such conditions include respiratory issues, heart attacks, strokes, and brain hemorrhages.

Accurate diagnosis of DoC can be challenging but is vital, especially in the early stages following a brain injury. Comprehensive clinical assessments, including evaluations such as EMG, EEG, evoked potentials, and PCI scores, can aid in this process.

Several characteristics of DoC provide insight into potential recovery outcomes, supported by moderate evidence:

Individuals in a minimally conscious state (MCS) typically have a more promising outlook for recovery compared to those in a vegetative state (VS). Additionally, patients with TBI generally show better recovery prospects than those with non-TBI.

A longer duration in a DoC is associated with a reduced likelihood of recovery compared to more recent brain injury cases.

For DoC stemming from any cause, there is limited evidence for the following findings:

A greater chance of recovery one year after a brain injury when diagnosed with MCS compared to VS/UWS.

An increased risk of worsening disability over time when VS/UWS persists for more than a year.

In cases of severe brain injury from trauma, most individuals will regain consciousness but with severe disability, necessitating ongoing care and assistance with basic activities.

1.3.3 Brain Death

Historically, the prevailing notion of death centered on the cessation of cardiorespiratory function. This view, rooted in the belief that the loss of respiration and circulation precedes the decline in brain function, was widely accepted.

In the 1950s, advancements in life support techniques, including cardiopulmonary resuscitation (CPR) and positive pressure ventilation (PPV), challenged the traditional definition of death, casting doubt on the interdependence of bodily functions. The concept of brain death, also known as death by neurologic criteria (BD/DNC), emerged when neurologists began to propose that neurological function held equal,

if not greater, significance than cardiorespiratory function in defining death.

The Harvard Brain Death Criteria, established in 1968, was the first clinical definition of brain death and included both clinical and EEG criteria. The Uniform Determination of Death Act, introduced in 1980, provided the legal foundation for neurological determination of death in the United States. Adult guidelines were later established in 1995 and revised in 2010 by the American Academy of Neurology (AAN). The American Academy of Pediatrics released guidelines for determining brain death in children in 1987, which were updated in 2011.

To comprehend the essence of brain death, it is necessary to explore its evolution and the associated controversies. Debates often revolve around terminology, such as "whole brain death" or "brainstem death." To promote understanding, experts widely recommend using the term BD/DNC.

Advocates of neurologic criteria for diagnosing brain death argue that the human body transcends its individual parts, asserting that death equates to the loss of the entire person. The brain, as the principal architect of the body and controller of vital functions, is attributed with a higher concept of personhood.

Opponents of BD/DNC have historically raised objections, asserting that brain death primarily serves to facilitate organ donation and can be inconsistent with perceived signs of life in some cases. Skeptics have questioned the diagnosis of brain death in the presence of persistent neurological function or undamaged brain regions.

Currently, there are multiple interpretations of BD/DNC:

- **Whole brain death** posits that severe damage must affect all key brain structures (hemispheres, diencephalon, brainstem, and cerebellum). This interpretation is supported by the United States and most other countries with national brain death standards and typically does not mandate the loss of neuroendocrine function.
- **Brainstem death** is recognized in the United Kingdom and several other countries. From this standpoint, the death of the brainstem alone is considered equivalent to human death, as the brainstem contains the centers responsible for consciousness and essential cardiac and respiratory functions.
- **Higher brain** formulation suggests that the destruction of the higher brain, including the cortex and bilateral hemispheres, suffices for diagnosing BD/DNC, given their critical role in cognition. However, this formulation contradicts

traditional BD/DNC criteria, as individuals with a loss of higher brain function can still breathe.

Clinically, distinguishing between "whole brain" and "brainstem" interpretations of death may seem inconsequential. In most cases of severe brain injury, whether due to various causes, irreversible brainstem damage follows a primarily supratentorial lesion.

Brain death can occur when the influx of blood or oxygen to the brain is interrupted. Amongst the possible causes, are: cardiac arrest, heart attack, stroke, blood clots, severe head injuries, brain hemorrhages, infections like encephalitis, brain tumors, respiratory issues, or other medical conditions.

Diagnosing brain death primarily depends on clinical assessment. If a thorough clinical examination, which includes two evaluations of brainstem reflexes and a single apnea test, definitively confirms brain death, further testing is not required.

Chapter 2

State of art

The following chapter will go into more detail about the study of coma, dealing in particular with the methods associated with the recording of the electroencephalographic signal and its analysis, to obtain indicators capable of predicting whether or not the patient will return to a state of conscience.

2.1 Why this field of study?

In addition to purely knowledge-oriented purposes, this area of study proves to be of great importance to healthcare costs.

According to a 2020 German study [35] based on data collected between 2015 and 2017 in Germany, the average duration of LOS (length of stay) of patients in a coma due to TBI (traumatic brain injury) was approximately 8 days and increased along with the extent of the trauma suffered.

The average cost at the hospital level was €11,918, of which 66% was due to admission, 13% to surgery, 7% to radiology, 5% to other laboratory tests and the remaining 9% to other hospital expenses. In the study, it was observed that the increase in the average cost was significantly contributed by a minority of patients suffering from serious and very serious TBIs, the same minority having the highest mortality within 6 months (66.7% for very serious and very serious TBIs). 57.7% for severe TBI). Considering the limited number of resources available to hospital facilities and the need to optimize them, researchers began to ask themselves how they could try to predict which patients could achieve a positive outcome. Among the possible methodologies taken into consideration in order to achieve this objective, one that has given encouraging results is the analysis of EEG signals.

2.2 Scales to evaluate awarness [20]

In order to efficiently evaluate the patient's status, numerous assessment scales have been created. They were created based on some main features such as: inter-rater reliability, ease of use, predictive value, and reproducibility. Four scales will be introduced below: Glasgow Coma Scale (GCS), Reaction Level Scale (RLS85), Full Outline of UnResponsiveness (FOUR) score, and Cerebral Performance Category (CPC) score.

The GCS is the most recognized and widely accepted coma rating scale, used for rapid pre-hospital assessment, evaluation of disease severity, prediction of morbidity and mortality prognosis, and management of comatose patients, and it has been incorporated into various trauma assessment systems. It has limitations in its usefulness for children younger than 3 years of age and before language acquisition. To overcome this problem a pediatric GCS has been developed, but its reliability has not yet been sufficiently proven. Another important limitation of the GCS is the unreliability of the score associated with patients with fixed and dilated pupils (they are evaluated as more serious than they are). The GCS is based on three components: eye-opening, verbal response, and motor response, with each component being assigned a score of up to 4-5 based on the observed response, and the values are then summed.

RLS85 is a scale that, albeit more difficult to learn, has proven utility and benefits but it is used almost exclusively in Scandinavia. The RLS85 is used to evaluate the clinical course of patients in coma and is considered a reliable tool for assessing its severity. Its limitations are the lack of information relating to reliability and low popularity. Similarly to the GCS it is based on the same three components (eye opening, verbal response, and motor response), which are assigned scores from 1 to 5 where the level of consciousness measured increases with the numerical value assigned.

FOUR is a coma rating scale that is gradually becoming more widely used. It is particularly useful for patients with fluctuating consciousness, as it captures changes in their neurological status over time. It is designed to evaluate the depth and duration of coma, as well as the presence of brainstem reflexes and breathing patterns. It is considered a complete and reliable tool for the evaluation of patients with altered levels of consciousness. Compared to other rating scales it is considered easier to learn to use. Four components are assessed in the FOUR

scales: ocular response, motor response, brainstem reflex, and respiration. Each component is associated with a score from 1 to 4 where a higher score implies a higher level of consciousness.

The Cerebral Performance Category (CPC) score is a commonly used scale for assessing neurological outcomes following cardiac arrest, ranging from recovery from a coma to brain death, evaluating both functional status and quality of life, with a final outcome scored from 1 to 5, where 1 indicates good brain performance and 5 indicates brain death. [3]

In addition to assessing consciousness, evaluating the long-term outcome of the patient is crucial. The Glasgow Outcome Scale (GOS) is the scale used for this purpose in the patients whose EEG data are analyzed in this thesis. The GOS categorizes patients into five levels based on their functional recovery, ranging from death to good recovery. Assessing the degree of disability or independence a patient achieves after the acute phase is important, as it provides valuable insights into long-term prognosis and quality of life.

2.3 Data acquisition tempistics

Having already discussed the importance of the electroencephalographic signal, it is important to know when these data are extracted. Since the ultimate goal of this type of study is to find a way to predict a patient's eventual awakening from a coma, the signal of interest is normally taken from when the patient is admitted until the first few days (normally within 24 hours from admission, but in some studies it can reach up to 72 hours). Obviously, to verify whether a predictive method is reliable it requires validation. To this end, the outcome of the patients whose signal was taken is recorded in the form of a value belonging to a scale such as the GCS. Recording is carried out in the majority of studies viewed 3 or 6 months after hospitalization.

2.4 Outcome prediction methodologies

Various studies have been carried out to try to predict the patient's outcome, among these some have used the EEG signal acquired in the absence of external stimuli, others have been based on the auditory evoked potential (or other evoked potentials) and still others have made use of neural networks.

Employing neural networks for prediction without needing preselected features is both the simplest and the most problematic method. On one hand, this approach often produces promising outcomes because neural networks can learn patterns directly from the raw data. The network can discern patterns that facilitate accurate predictions by examining an extensive collection of acquired signals and corresponding patient outcomes. However, a significant drawback of this technique is its "black box" characteristic: although the network can make reliable predictions, it offers little insight into the processes it uses to arrive at those predictions, which complicates efforts to understand and analyze the underlying predictive mechanisms.

Prediction via auditory discrimination occurs by observing this particular type of evoked potential. Several studies have been able to ascertain that subjects in whom there is an improvement in the ability to distinguish sounds during the early stages of coma are more likely to have positive outcomes (intended as awakening or survival) within 3 months. In particular, it has been noted that the deterioration of this ability is common in patients who do not survive.

In predictions based on EEG (without EPRs), different patterns or indicators are taken into account which, based on studies, have been classified as favorable or unfavorable. For example, continuous pattern, diffusely slowed (a continuous pattern with a dominant frequency strictly less than 8 Hz), or normal (a continuous pattern with a dominant frequency greater than or equal to 8 Hz) are considered favorable patterns, while isoelectric, low-voltage, or burst-suppression with identical bursts (bursts that are identical to each other and have interburst intervals of at least one second occurring either without activity or with low-voltage activity present) as unfavorable patterns.

2.5 Examples of studies on prediction based on various methods

This section reports seven examples of studies focused on the use of EPR to predict the outcome of a patient in a coma.

2.5.1 First Example [22]

This study aims to use raw EEG data to train and validate a convolutional neural network (CNN)-based classifier for predicting neurological outcomes in patients with postanoxic encephalopathy after cardiac arrest, particularly focusing on assessments made 12 hours after cardiac arrest. The different classes are based on the Cerebral Performance Category (CPC) scale.

The EEG signals for this study were recorded using 21 channels at a frequency of 256 Hz, from 12-24 hours post-cardiac arrest to 5 days thereafter. The patients' outcomes were assessed 6 months later using the CPC, with scores of 1-2 classified as 'good' and scores of 3-5 classified as 'poor'.

The EEG signals were filtered within a 0.5-35 Hz frequency range, down-sampled to 64 Hz, and re-referenced using a longitudinal bipolar montage. Training and validation of the CNN utilized 5-minute segments of clean EEG data recorded at 12 and 24 hours post-cardiac arrest. These segments were split into 10-second, non-overlapping intervals, creating 30 fragments per time point for each patient. Data from 80% of the patients were employed for training the network, while the remaining 20% were reserved for validation. The outcome probability for each patient at a given time was derived from the average probability of the 30 snippets within the 5-minute segment. The network was built using Python with Keras and Theano, and ran on a CUDA-enabled NVIDIA GPU (GTX-1080) on a CentOS 7 system. The Adam optimizer was used for stochastic optimization with parameters: learning rate of 0.00002, $\beta_1 = 0.91$, $\beta_2 = 0.999$, and $\epsilon = 1 \times 10^{-8}$. Categorical cross-entropy was used as the loss function, and the final output was a binary classification of 'good' or 'poor', reported in terms of sensitivity and specificity.

The CNN training process took around 50 minutes to complete and the predictions were more accurate at 12 hours post-cardiac arrest compared to 24 hours, with an AUC of 0.89 versus 0.76 in the validation set. In the validation, effectuated with an independent dataset, the model achieved a sensitivity of 58% and a specificity of 100% for predicting poor outcomes at 12 hours post-cardiac arrest, while, for

predicting good neurological outcomes, the sensitivity was 58% with a specificity of 97%.

2.5.2 Second Example [34]

This study aims to present a general method for decoding stimulus categories on a single-trial basis, with the objective of reducing prior assumptions. In particular, the proposed method, through a data-driven approach, manages to estimate the onset and duration of the effect of interest, allowing to optimize the use of the measured voltage. The scalp voltage topography of the electroencephalographic signal appears to contain information pertaining to the stimuli perceptible at the single-trial level and usable for decoding. A topographic clustering model, the Gaussian Mixture Model (GMM), is applied to separate the stimulus categories and classify which condition their sets of single-trials belong to. This multivariable decoding method enables the identification of crucial voltage patterns and their associated timings that differentiate the functional characteristics between the two experimental conditions.

The topography consists of a series of voltage values recorded from the electrodes at each moment in time. Subsequently, each topography is normalized using its instantaneous Global Field Power (GFP), ensuring that the classification algorithm relies solely on the topography's shape. A GMM probability distribution is then used to reduce the numerous topographies into a few but more meaningful template maps. In order to estimate the GMM distribution, an expectation-maximization procedure is used which, by iterating the estimates of the model parameters (such as priors, means and covariance matrices), maximizes the probability and decreases the functional error. The covariance matrices used in this algorithm are initially obtained by considering the topographies of the clusters estimated by a k-means clustering algorithm. Due to the small size of the training set in this study, the covariance matrices were limited to being exclusively diagonal. The GMM model is applied to each condition separately, thus resulting in one model for each condition. The number of Gaussians was assumed as a prior hypothesis. Each Gaussian is linked to a specific topography from the original dataset using the GMM model.

Since the misclassification error and the posterior probability are inversely proportional, the latter is calculated to minimize the former. Furthermore, posterior probabilities, rearranged according to their original temporal order, are used to study stimulus-related information. It follows that in the various trials there is a time series of posterior probabilities for each template map.

The posterior probabilities of the model and dataset are calculated for both conditions, in order to identify discriminative time periods between them. It is used the Bayes Factors (BF) to identify when the model best explains that condition. They can be calculated at each latency and for each trial, allowing to assign a specific observation to the template map of one of the models.

The number of Gaussians of the two models is decided by taking into account the average performance of the classification along the ten divisions in the cross-validation procedure. The performance of classification in cross-validation is calculated by manipulating the threshold of the discrimination function and evaluating the area underwritten by the ROC curve. Having two conditions and ten splits gives twenty areas under the curve (AUC) values. This procedure is not carried out for single trials but is carried out for trials or sub-set trials.

2.5.3 Third Example [18]

This study aims to improve the ability to predict the outcome of post-cardiopulmonary resuscitation coma by increasing the accuracy of EEG assessments. To achieve so, this research investigates the combined use of background EEG patterns and EEG reactivity (EEG-R) to improve predictive sensitivity and specificity.

The study involved 160 comatose patients post-CPR who were between 18 and 80 years old, in a coma for at least 24 hours post-CPR with a GCS score \leq 8, and undergoing assessment during normothermia; but who were not: using central nervous system inhibitors, terminally ill, or in a state of peripheral neuropathy. EEG was performed through the standard electrode placements, using a 32-channel digital system, with recordings lasting at least 30 minutes. The acquired signals were interpreted by two certified physicians, with discrepancies resolved by senior EEG experts. Follow-up was conducted 3 months post-coma via phone interview, using the Glasgow Outcome Scale (GOS) to classify outcomes as awakening (GOS 3-5) or non-awakening (GOS 1-2).

Statistical analyses were performed using SPSS version 21.0. Continuous variables were analyzed using t-tests or Mann-Whitney U tests, while categorical variables were assessed with chi-squared tests. Consistency of EEG interpretation was measured using the Kappa test, and receiver operating characteristic (ROC) curves were used to determine the best cut-off values for predicting recovery. Amongst the studied metrics were present specificity, sensitivity, positive predictive value (PPV), and negative predictive value (NPV).

62 (38.75%) of the 160 patients awakened within 3 months. The awakening group had a significantly higher median GCS score compared to the non-awakening group ($P=0.000$), and the ROC analysis showed an area under the curve of 0.708 ($P=0.000$) for GCS, with an optimal cut-off value of 3.5 for predicting awakening.

EEG patterns classified as slow wave or continuous patterns (category I) were more prevalent in the awakening group, with the slow wave pattern (category I) appearing in 61.3% of the awakening group compared to 19.4% in the non-awakening group. Significant differences were observed in the proportions of category Ia and Ib patterns between the two groups ($P=0.000$ and $P=0.076$, respectively). Inter-rater reliability for EEG interpretation was high ($Kappa=0.864$, $P=0.000$).

Among the EEG patterns, the slow wave pattern was the most accurate in predicting awakening, achieving 73.1% accuracy, 61.3% sensitivity, and 80.6% specificity. The sensitivity was higher for the slow wave pattern compared to the Ia and Ib patterns and was superior to GCS in specificity. EEG assessments performed at different time points showed that the slow wave pattern within 8-14 days post-coma provided the highest accuracy (100% sensitivity and specificity).

Those results suggest that EEG grading, especially within the time period of 8-14 days, offers valuable prognostic information and should be considered in clinical decision-making.

2.5.4 Fourth Example [28]

This study aims to evaluate the prognostic significance of single EEG patterns in postanoxic comatose patients, defined according to the ACNS terminology, and to analyze how their predictive value changes during the first 12-72 hours after cardiac arrest (CA). The 211 patients whose signals have been used in this study were treated with mild endovascular therapeutic hypothermia (TH), with their core temperature maintained at 32-34°C for 24 hours. This study excluded the patients whose TH was interrupted, who didn't show an EEG within 72 from CA, whose CA had non-cardiac origin, who presented intra-operative CA, who suffered from other severe neurological injuries, and ones who had severe extra-neurological pathology with a life expectancy under six months.

The acquisition of the EEG recordings started as soon as possible after the patients were admitted to ICU, and were classified based on the time that intercurred between the CA and the signal acquisition, falling under four possible time-frames: 12 hours, 24 hours, 48 hours, and 72 hours.

EEGs were classified either based on ACNS terminology, focusing on continuity, voltage, and reactivity, or taking into account burst suppression with identical bursts at 12 and 24 hours. Recordings with ictal or periodic epileptiform activity were categorized separately.

An interviewer blind to the EEG finding assessed, using the Glasgow Outcome Scale (GOS), the neurological outcomes 6 months after cardiac arrest, categorizing as "good" (GOS 3-5) or "poor" (GOS 1-2).

To effectuate the statistical analysis, for each time-frame of every EEG pattern were calculated the following statistical indicators: sensitivity, specificity, positive predictive value (PPV), and negative predictive value (NPV).

Through this study was observed that continuous and nearly continuous patterns were only present in patients with good outcomes at 12 hours; by 24 hours, burst-suppression and isoelectric patterns were not observed in patients with good outcomes, and at 48 and 72 hours, only continuous, nearly continuous, and epileptiform discharges were seen in patients with good outcomes.

For poor outcomes, burst-suppression with highly epileptiform discharges and isoelectric patterns were observed at 12 hours; at 24 and 48 hours a variety of patterns, including burst-suppression and isoelectric, were linked to poor outcomes, and at 72 hours, suppression and isoelectric patterns signaled poor outcomes.

This study confirmed that specific EEG patterns can predict outcomes with high accuracy at different time points post-CA, bringing the example that continuous and nearly continuous patterns at 12 hours reliably predict good outcomes, while isoelectric and burst-suppression patterns predict poor outcomes from 24 hours onwards.

2.5.5 Fifth Example [10]

This study explores the potential of using high-density electroencephalography (EEG) to predict metabolic activity, diagnose states of consciousness, and forecast patient outcomes.

The patients taken into account in this study were either diagnosed with disorders of consciousness or they had emerged from such conditions and were compared

with a control group of healthy individuals.

Patients underwent assessments using: the Coma Recovery Scale-Revised when they did the PET and EEG evaluations (the diagnosis was based on the results from multiple CRS-R evaluations); the Glasgow Outcome Scale-Extended 12 months later (to determine patient outcomes). PET scans were analyzed to diagnose either complete hypometabolism or partial preservation of brain activity, which informed the diagnosis of PET-negative or PET-positive states.

High-density EEG signals were acquired during fluorodeoxyglucose (FDG) uptake using a 256-sensor electrode net and a sampling rate of 250 Hz or 500 Hz. Were analyzed data from 89 patients with disorders of consciousness. Among them, 11 patients emerged from a minimally conscious state (MCS), four had locked-in syndrome, and there were 26 control subjects.

The data were preprocessed to achieve artifact removal and decomposed into spectral components using the FieldTrip toolbox. After the preprocessing was calculated: power estimates (for delta, theta, and alpha frequency bands) and connectivity between EEG channels (using the debiased weighted phase lag index). The connectivity data was used to construct symmetrical matrices, which were then analyzed to calculate various network metrics such as participation coefficient, clustering coefficient, modular span, characteristic path length, and modularity.

The connectivity matrices were thresholded to retain significant connections and binarized for network analysis. Key topological characteristics of the networks were calculated across different scales, capturing both local and global properties of brain connectivity. Metrics were computed for each frequency band, resulting in a comprehensive set of 21 metrics per patient.

The study found that specific EEG network metrics correlated strongly with behavioral assessments and PET diagnoses and that these metrics also demonstrated prognostic value, accurately predicting long-term patient outcomes. This kind of assessment managed to identify patients misdiagnosed by clinical consensus, highlighting the potential of EEG metrics to complement traditional diagnostic methods and reduce misdiagnosis rates.

2.5.6 Sixth Example [32]

The study aims to assess the prognostic value of EEG features (of temporal, frequency, and spatial domains) collected with a limited frontoparietal montage for

comatose patients.

This retrospective study involved 81 comatose patients with acquired brain injuries (ABI) admitted to the ICU who satisfy the following criteria:

- GCS score of 7 or lower with specific subscale scores ($E=1$, $V\leq 2$, $M\leq 4$).
- EEG recordings using a frontoparietal montage (channels F3, F4, P3, P4) taken within four weeks of ICU admission and lasting at least 30 minutes.
- EEG monitoring starting at least 24 hours after the cessation of sedatives.
- Availability of 60-day Glasgow Outcome Scale (GOS) scores.
- No diagnosis of brain death before or during EEG monitoring.
- No return to consciousness during EEG monitoring.

The GOS scores split patients into two outcome-based classes: favorable outcome ($GOS \geq 3$) and unfavorable outcome ($GOS \leq 2$).

Continuous EEG recordings were acquired through a limited frontoparietal montage focused on four electrodes (F3, F4, P3, P4, and Cz as the reference), using a multi-lead device with a sampling rate of 250 Hz. The extracted features from these recordings comprised: the burst suppression ratio (BSR) in the time domain; the root mean square (RMS) in the time domain; the power ratio of θ to α rhythm (θ/α) in the frequency domain; and the phase-lag index (PLI) between F3 and P4 in the spatial domain.

The patients' data were analyzed using partial correlation to eliminate redundant factors and multiple correspondence analysis to explore group discrimination, while logistic regression was employed to develop EEG feature-based predictors.

For the overall patient group, increased BSR, reduced RMS, higher θ/α ratio, and lower PLI (F3, P4) were significantly associated with unfavorable outcomes, showing high area under the curve (AUC) values. Amongst the ones who suffered from strokes, notable features were BSR, RMS, ϑ/total , ϑ/δ , and PLI (F3, P4), while, amongst the TBI patients, only PLI (F3, P4) showed significance. The combined use of BSR and PLI (F3, P4) yielded the highest predictive accuracy.

The study managed to demonstrate that EEG features from a limited frontoparietal montage are valuable for predicting outcomes in comatose patients, highlighting the value that PLI (F3, P4) could bring.

2.5.7 Seventh Example [36]

This study aims to improve the diagnostic ability in cases of prolonged disorders of consciousness (pDOC) by analyzing the patient's brain connectivity using quantitative electroencephalography (qEEG), through the research of EEG markers capable of differentiating between pDOC patients and healthy controls.

Inclusion criteria required participants to have been unconscious for over 28 days, undergone multiple CRS-R assessments by professional doctors, had more than 12 hours of video EEG monitoring, completed a head MRI, maintained relatively intact intracranial structures without skull defects, and provided comprehensive clinical data, while exclusion criteria involved poor data quality due to significant artifacts, use of sedatives or anesthetics during data collection, and unstable vital signs. Nine healthy individuals were included as a control group.

Collected patient data included age, sex, primary disease, brain injury regions, and admission CRS-R scores. MRI scans were performed using a SIEMENS SKYRA 3T scanner, capturing 3D-T1-MPRAGE sequences with specific parameters (TR = 2000ms, TE = 3.0ms, slice thickness = 1mm, flip angle = 9°, slice gap = 50%, and resolution matrix = 256 × 256).

The EEG recordings were acquired with a sampling rate of 500 Hz using 21 Ag/AgCl electrodes positioned according to the international 10-20 system, while the participants remained relaxed with eyes closed during recording. The recordings were preprocessed by band-pass filtering (0.5-45 Hz) and using independent component analysis (ICA) to remove the artifacts.

The EEG power spectrum was analyzed using specialized data analysis tools. The DTABR ratio, defined as $\frac{\delta+\theta}{\alpha+\theta}$, was computed to evaluate the balance between slow and fast brain activities. Pearson's correlation coefficient was used to assess linear dependencies between EEG channels. Granger causality analysis was employed to evaluate directional interactions between brain regions, while phase transfer entropy (PTE) quantified information flow between EEG channels. Due to the non-normal data distribution, non-parametric tests were used to conduct statistical comparisons of EEG connectivity metrics between the pDOC group and the control group. To evaluate how effective the EEG connectivity measures were in

diagnostic were constructed the receiver operating characteristic (ROC) curves.

The study's results revealed that patients with prolonged disorders of consciousness (pDOC) showed significantly higher delta band power and lower alpha and beta band power compared to healthy controls, alongside an elevated DTABR ratio, indicating a shift towards slower brain activities. Pearson's correlation coefficients indicated higher connectivity in the delta, theta, and alpha bands within the pDOC group. Furthermore, Granger causality analysis identified reduced directional connectivity between hemispheres, and phase transfer entropy (PTE) values were lower across all frequency bands, suggesting decreased information flow.

Chapter 3

Methods

3.1 Dataset

The dataset includes EEG signals from thirteen patients who entered a coma following a traumatic brain injury (TBI). The signals were supplied already low-pass filtered at 30 Hz and resampled at 64 Hz.

Because of the important damage suffered by the patients often compromising the integrity of the cranium itself, the EEG signals were acquired taking into account 4 channels, corresponding to electrodes FP1, FP2, T3, and T4.

The thirteen patients belong to three different "classes". The classes are based on the patient's outcome measured through the Glasgow Outcome Scale.

The three classes correspond respectively to: GOS 1 (no awakening from coma and eventual death); GOS 3 (the patient awakens from coma, but suffers from severe disability with permanent need for assistance); GOS 5 (the patient awakens from coma, fully recovers or suffer from minor disability with resumption of normal life).

3.2 Preprocessing

The first step carried out in the signals preprocessing is high-pass filtering of the signals at 0.5 Hz using a fifth-order butter filter. This filter application has the task of alleviating low-frequency noise. The cut-off frequency was chosen so as to preserve all the bands of interest in the EEG signal.

The successive step to the high-pass filtering was the removal of the artifacts due to the detachment of the electrodes. This process was carried out through visual removal assisted by a function that flags a sequence of spikes of an amplitude not congruent with brain activity. The removal of the flagged part of the signal was carried out in all four channels so that the time intervals represented are always

the same regardless of the channel of the same patient.

Assuming that the assumption of stationarity of the comatose patient in a time span of 5 seconds is valid, it was decided to divide the signals into epochs of 5 seconds.

To increase the dataset's numerosity, a data segmentation technique was implemented, dividing the original dataset into 20 separate datasets. In 19 out of the 20 datasets, each represented 50 minutes of the EEG trace, split into 600 epochs, while Dataset 7 contained only 40 minutes of data.

Datasets 1 through 7 included signals from all 13 patients. However, in Datasets 8 and 9, no signal from the 11th patient was included due to the shorter length of their EEG trace. In Dataset 10, signals from both the 1st and 11th patients were excluded for the same reason. The 2nd patient's signal was additionally excluded in Datasets 11 through 14, the 9th patient's in Datasets 15 through 17, and the 12th patient's in Datasets 18 through 20. The segmentation process was halted after 20 datasets to avoid creating datasets with only one patient in a class.

3.3 Indicators Extraction

A total of 17 indicators were calculated: 12 of connectivity and 5 of non-connectivity. Their descriptions that will be reported in this section are based on [5], [12], [27], and [8]

The indicators of connectivity are:

- **Spectral Coherence:** it measures the degree of consistency or coupling between two signals across different frequency bands in the spectrum. Spectral coherence can range from 0 to 1, where higher values indicate stronger coupling or greater consistency between signals in the considered frequency bands. Spectral coherence is used to evaluate functional connectivity or synchronization between different brain regions, which can be related to cognitive, behavioral, or pathological processes. It helps in identifying how brain regions communicate with each other over various frequencies.

$$C_{xy}(f) = \frac{|S_{xy}(f)|^2}{S_{xx}(f) S_y(f)}$$

where $S_{xy}(f)$ is the cross-spectral density between signals x and y , and $S_{xx}(f)$ and $S_{yy}(f)$ are the power spectral densities of x and y , respectively.

- **Phase Coherence:** It measures the temporal consistency of the relative phases between two signals. Phase coherence can range from 0 to 1, with higher values indicating greater consistency or synchronization of relative phases between signals. Phase coherence is used to evaluate temporal synchronization or communication between different brain regions, which can be related to information processing and neural integration processes. It is essential for understanding the timing relationships in neural oscillations.

$$\gamma_{xy}(f) = \frac{|\langle e^{j(\phi_x(f)-\phi_y(f))} \rangle|}{\langle |e^{j\phi_x(f)}| \rangle \langle |e^{j\phi_y(f)}| \rangle}$$

where $\phi_x(f)$ and $\phi_y(f)$ represents the phases of signals x and y at frequency f .

- **Amplitude Coherence:** it assesses how well the relative amplitudes between two signals match or remain consistent. Amplitude coherence can range from 0 to 1, with higher values indicating greater consistency or synchronization of relative amplitudes between signals. Amplitude coherence is used to evaluate the coupling or synchronization of activity intensities between different brain regions, which may be related to information processing or pathological phenomena. This measure is particularly useful in detecting amplitude-based synchronization.

$$\text{Amplitude Coherence} = \frac{\sum_t A_x(t)A_y(t)}{\sqrt{\sum_t A_x(t)^2} \sqrt{\sum_t A_y(t)^2}}$$

where $A_x(t)$ and $A_y(t)$ are the amplitudes of signals x and y at time t .

- **Partial Directed Coherence (PDC):** it is a measure of partial directional connectivity between two signals, taking into account the influences of other signals in the system. PDC values range from 0 to 1, with higher values indicating greater directionality or flow of information from one signal to another. PDC provides information about the direction of information flow between different brain regions, indicating which regions influence others in a dynamic system. It helps in understanding causal relationships in multivariate data.

$$PDC_{ij}(f) = \frac{A_{ij}(f)}{\sqrt{\sum_{k=1}^N |A_{ik}(f)|^2}}$$

where $A_{ij}(f)$ is the element of the Fourier transform of the model coefficients matrix.

- **Mutual Information (MI):** it quantifies the joint entropy between two signals, indicating the amount of information shared between them, with values ranging from 0 to ∞ where higher values denote a greater degree of shared information or correlation between the signals. MI measures the correlation or dependence between different brain regions, reflecting neural processes related to cognitive or pathological states, and quantifies how much information about one signal can be inferred from another.

$$MI(X, Y) = H(X) + H(Y) - H(X, Y)$$

where $H(X)$ and $H(Y)$ represents the marginal entropies of the considered vectors X and Y , and $H(X, Y)$ denotes their joint entropy.

- **Phase Locking Value (PLV):** it is a measure of the phase coherence between two signals in a given frequency range. PLV values range from 0 to 1, with higher values indicating greater coherence or synchronization of relative phases between signals. The PLV provides information on the temporal synchronization of relative phases between signals, indicating the temporal coherence of recorded brain activities. This measure is crucial for assessing phase synchronization in oscillatory brain activities.

$$PLV = \frac{1}{N} \sum_{n=1}^N e^{j\Delta\phi_n}$$

where $\Delta\phi_n$ is the phase difference between the two signals at time n .

- **Phase Lag Index (PLI):** it is a measure of the asymmetric phase coherence between two signals, evaluating the consistency of the phase differences between the signals. PLI values range from 0 to 1, with higher values indicating greater asymmetry in the distribution of phase differences between signals. PLI provides information on the directionality of communication or synchronization between brain regions, highlighting connections that show consistent asymmetry in the relative phase.

$$PLI = \frac{1}{N} \sum_{n=1}^N \text{sign}(\sin(\Delta\phi_n))$$

where $\Delta\phi_n$ is the phase difference between the two signals at time n .

- **Phase Slope Index (PSI):** it is a measure of high temporal resolution phase coherence between two signals, evaluating the directionality of communication based on rapid changes in relative phase. PSI values range from 0 to

1, with higher values indicating greater short-term phase coherence between signals. PSI provides information about the directionality of communication or synchronization between brain regions, focusing on rapid changes in the relative phase between signals.

$$\text{PSI} = \frac{\Delta\phi}{\Delta f}$$

where $\Delta\phi$ represents the phase difference and Δf defines the frequency difference.

- **Directed Transfer Function (DTF):** it measures the direction of information transfer between two signals, indicating the extent of information flow across different frequencies. With values ranging from 0 to 1, higher scores reflect stronger directionality and information transfer between signals in specific frequency bands. It highlights the frequency bands where significant information flow occurs between brain regions.

$$\text{DTF}_{ij}(f) = \frac{H_{ij}(f)}{\sqrt{\sum_{k=1}^N |H_{ik}(f)|^2}}$$

where $H_{ij}(f)$ represents the element of the transfer matrix derived from the Power Spectral Density.

- **Phase Transfer Function (PTF):** it is a measurement of the phase relationship between two signals, evaluating the phase difference between signals at different frequencies. PTF values range from $-\infty$ to $+\infty$ indicating the relative phase difference between signals at different frequencies. PTF provides information on the phase relationship between two signals, highlighting the relative phase difference in different frequency bands.

$$\text{PTF} = \frac{\phi_{ij}(f)}{\Delta f}$$

where $\phi_{ij}(f)$ represents the phase difference, and Δf defines the frequency difference.

- **Power Correlation:** it measures the statistical relationship or dependence between the amplitudes of two signals by evaluating their power correlation. Power Correlation values range from -1 to 1, where positive values indicate positive correlation, negative values indicate negative correlation, and a value of zero indicates no correlation. A positive correlation means that when the amplitude of one signal increases, the amplitude of the other signal also tends

to increase, and vice versa. In contrast, a negative correlation means that as the amplitude of one signal increases, the amplitude of the other signal tends to decrease.

$$\text{Power Correlation} = \frac{\sum_{i,j} \text{Corr}(P_i, P_j)}{N}$$

where P_i and P_j are the power spectra of signals i and j , and N is the number of signals.

- **Granger Causality:** it is a statistical method used to determine the causal relationship between two signals by assessing whether one signal can predict the future values of another signal. Granger Causality values range from 0 to 1, with higher values indicating greater evidence of causality from one signal to another. Granger Causality provides information on the direction and strength of causality between two signals, based on the predictive ability of one signal over the other.

$$X \text{ causes } Y \text{ if } \text{Var}(Y | Y_{\text{past}}) > \text{Var}(Y | Y_{\text{past}}, X_{\text{past}})$$

where $\text{Var}(Y | Y_{\text{past}})$ is the variance of Y given its past values, and $\text{Var}(Y | Y_{\text{past}}, X_{\text{past}})$ is the variance of Y given its past values and the past values of X .

The indicators of non-connectivity are:

- **Rhythm Power:** it refers to the energy distribution of the EEG signal in different frequency bands, such as delta, theta, alpha, beta, and gamma. The power of the rhythms characterizes brain activity and identifies anomalies or distinctive patterns associated with different conditions. The total spectrum sums to 100% of the signal power, while the ratio between the power of each band and the total spectrum provides the relative powers of the rhythms.

$$P_{\text{rhythm}} = \frac{\sum_{f \in \text{band}} P(f)}{\sum_f P(f)}$$

where $P(f)$ is the power at frequency f , and the band corresponds to the specific rhythm frequency range.

- **Median Frequency:** The median frequency is the frequency at which half of the signal's spectral energy is below it and half above it. It provides an estimate of the dominant or prevalent frequency in the EEG signal. This is important for understanding the central frequency of recorded brain activity,

which can vary based on mental state, age, physiological conditions, and pathologies. It is calculated by identifying the frequency where the partial cumulative power spectral density (PSD) equals half of its total cumulative.

$$\text{Median Frequency} = f_{\text{median}} \quad \text{such that} \quad \sum_{f=0}^{f_{\text{median}}} P(f) = \frac{1}{2} \sum_{f=0}^{f_{\max}} P(f)$$

where $P(f)$ represents the power at frequency f , and f_{\max} is the maximum frequency.

- **Root Mean Square (RMS):** it is a measure of overall signal strength, calculated as the square root of the mean of the squares of the signal values. It assesses the average amplitude of the EEG signal and is linked to various aspects of brain activity, including neuronal activation and the intensity of the brain's response to external stimuli.

$$\text{RMS} = \sqrt{\frac{1}{N} \sum_{i=1}^N x_i^2}$$

where x_i represents the signal values and N denotes the number of samples.

- **Entropy:** it is a measure of the complexity or uncertainty of a probability distribution. In EEG signal analysis, entropy is derived from the probability distribution of signal values. Higher entropy indicates greater randomness and disorganization, while lower entropy (minimum 0) signifies more regularity and predictability. It evaluates the complexity of brain activity, offering insights into its dynamics and identifying unique patterns

$$H(X) = - \sum_{i=1}^N p(x_i) \log p(x_i)$$

where $p(x_i)$ is the probability of the signal value x_i .

- **Hurst Exponent:** it quantifies the persistence or long-term memory of a stochastic process. In the context of EEG signals, the Hurst exponent can be used to evaluate the regularity or persistence of fluctuations in the signal over time. The Hurst exponent can range from 0 to 1, where values closer to 1 indicate greater persistence in the signal, and values closer to 0 indicate greater randomness or random fluctuations in the signal. It is particularly

useful in analyzing long-term EEG signals to evaluate the persistence of patterns or trends over time. It is calculated using the rescaled range analysis.

$$H = \frac{\log \frac{R/S}{n}}{\log(n)}$$

where R is the range of the cumulative deviations from the mean, S is the standard deviation, and n is the number of data points.

3.4 Statistical Metrics

To analyze the extracted indicators, statistical metrics were initially calculated, focusing on parameters such as mean, median, mode, percentiles, minimum and maximum values, standard deviation, variance, skewness, and kurtosis. Following the calculation, a visual inspection was performed, highlighting standard deviation, variance, skewness, and kurtosis as the most significant metrics. Due to the strong correlation between variance and standard deviation, only the standard deviation was considered for further analysis. Consequently, the focus will be on standard deviation, skewness, and kurtosis in subsequent evaluations. Their descriptions are based on [21], [30].

- **Standard Deviation:** it quantifies the degree of variation or dispersion within a set of values. It reflects how much individual data points differ from the mean of the dataset. A low value of standard deviation means that the data points tend to be close to the mean, whereas a high one indicates that the data points are spread out.

$$\sigma = \sqrt{\frac{1}{N} \sum_{i=1}^N (x_i - \mu)^2}$$

where σ is the standard deviation, N is the number of values, μ is the mean of the values, and x_i is each individual value.

- **Kurtosis:** Kurtosis is a statistical measure that describes the shape of the tails of a distribution compared to a normal distribution. If kurtosis is zero, the tail shape is similar to a normal distribution; if it is greater than zero, the

distribution has heavier or longer tails indicating the presence of outliers; if less than zero, the distribution has lighter or shorter tails indicating a flatter distribution.

$$\text{Kurtosis} = \frac{\sum_{i=1}^N \frac{x_i - \mu}{\sigma}^4}{(N-1)(N-2)(N-3)} - \frac{3(N-1)^2}{(N-2)(N-3)}$$

- **Skewness:** it is a measure that indicates the asymmetry of the distribution of values in a data set. A skewness greater than zero signifies a distribution with a longer or fatter right tail and data concentrated on the left, while a skewness less than zero indicates a longer or fatter left tail with data concentrated on the right; when its value is zero it represents a symmetric distribution.

$$\text{Skewness} = \frac{\sum_{i=1}^N \frac{x_i - \mu}{\sigma}^3}{(N-1)(N-2)}$$

3.5 Features Selection

The features taken into consideration in this study are the statistical metrics of the indicators. Specifically, any indicator's statistical metrics (except the one where the metrics were not calculated like the Granger Causality) were associated with as many features as the number of channels (except the coherence where have been taken into account the 6 possible combinations). The first part of the feature selection was focused on the individuation of the most significant indicator-statistical metric combination. This process was executed in two different ways: the non-standard-functions-based (NSF-based) selection, and the standard-functions-based (SF-based) selection.

- NSF-based feature selection was performed using custom functions that employed a traditional top-down approach, designed to work with groups of features rather than individual ones.
- SF-based selection was carried out using pre-existing functions available in Matlab.

3.6 Classification

In order to verify the validity of the selected parameters it was decided to use them in a classifier. The ones employed in this study are Fisher's linear discriminant, Decision tree, K-Nearest Neighbors (K-NN), and Support Vector Machine (SVM). The following descriptions are based on [15] and [4].

Because the previously used dataset was not fit for the training of a model, it was decided to use that data to make a new one.

After the removal of the electrode detachment artifacts, every signal was split into many smaller signals with a length of 204'800 samples (50 minutes * 60 seconds * sampling rate). Those signals were then split into epochs of 320 samples (5 seconds * sampling rate) and reassembled in 20 Datasets.

For every signal, wherever it was possible, were calculated: standard deviation, variance, skewness, and kurtosis of each indicator; and they were memorized in a struct of features, to assemble them when needed.

3.6.1 Fisher's Linear Discriminant (FLD)

Fisher's Linear Discriminant (FLD) is a classification technique that separates classes by identifying a linear combination of features that maximizes class distinction. The procedure begins with calculating the mean and variance of each feature within each class; and then continues computing two matrices: the within-class scatter matrix S_W , which quantifies the spread of data points within each class, and the between-class scatter matrix S_B , which is a measure of the variance between the class means.

The objective of FLD is to find the optimal direction for projecting the data to achieve the greatest separation between classes. This involves solving an optimization problem to maximize the Fisher criterion, expressed as:

$$J(\mathbf{w}) = \frac{\mathbf{w}^T S_B \mathbf{w}}{\mathbf{w}^T S_W \mathbf{w}}$$

where \mathbf{w} denotes the direction of projection. The Fisher criterion aims to maximize the separation between class means while minimizing the variance within each class. To determine this optimal direction, the generalized eigenvalue problem is solved:

$$S_W^{-1} S_B \mathbf{w} = \lambda \mathbf{w}$$

The direction of the optimal projection is represented by the eigenvector associated with the largest eigenvalue, and allows, by projecting the data onto it, to reduce the dimensionality and enhance class separability. Classification is then performed by applying a threshold to the projected data.

Pros:

- **Dimensionality Reduction:** FLD effectively reduces dimensionality while maintaining class separation by finding a linear projection that maximizes class distinction.
- **Computational Efficiency:** It is computationally efficient, especially for datasets with fewer features.

Cons:

- **Assumption of Linearity:** FLD relies on the assumption of linear separability and equal class covariances, which may not be valid for complex datasets.
- **Sensitivity to Outliers:** It can be affected by outliers, which might distort the estimated means and variances.

It was obtained by using the Matlab function `fitcdiscr(data, labels, 'DiscrimType', 'pseudoLinear')` from the Statistics and Machine Learning Toolbox.

3.6.2 Support Vector Machine (SVM)

Support Vector Machines (SVM) are classifiers used for various tasks, including classification, regression, and outlier detection. The primary concept behind SVM is to find the hyperplane that optimally separates the data into distinct classes. For linear SVM, this hyperplane is determined by maximizing the margin, which is the distance between the hyperplane and the closest data points from each class, known as support vectors.

Mathematically, for a set of training data $\{(\mathbf{x}_i, y_i)\}$, where \mathbf{x}_i is the feature vector and y_i is the class label, SVM solves:

$$\min_{\mathbf{w}, b} \frac{1}{2} \|\mathbf{w}\|^2$$

subject to:

$$y_i(\mathbf{w}^T \mathbf{x}_i + b) \geq 1 \quad \text{for all } i$$

In scenarios where data is not linearly separable, SVMs use kernel functions to map the data into higher-dimensional spaces, where linear separation is feasible. Some of the most used kernels are radial basis function (RBF), polynomial, and sigmoid kernels.

Pros:

- **High-Dimensional Suitability:** SVM is effective in high-dimensional spaces and handles cases where the number of features is large relative to the number of samples.
- **Kernel Flexibility:** Kernels enable SVM to capture non-linear relationships by transforming the data into higher-dimensional spaces.

Cons:

- **Computational Intensity:** SVM can be computationally intensive, particularly with large datasets or complex kernels.
- **Parameter Tuning Challenges:** The performance of SVM is highly dependent on the choice of kernel and parameter settings, which can be difficult to optimize.

It was obtained by using the Matlab function fitcecoc(data, labels) from the Statistics and Machine Learning Toolbox.

3.6.3 Decision Tree

Decision Trees are used for regression and classification tasks. They function by splitting the data into subsets based on feature values, resulting in a tree-like structure of decisions. Each node represents a test on an attribute, each branch shows the result of the test, and each leaf node signifies a final decision or predicted value.

The tree is constructed by selecting the attribute that best divides the data based on criteria such as Information Gain, Gini Index, which are employed for classification tasks, or Variance Reduction which is used for regression.

Pros:

- **Ease of Interpretation:** Decision Trees offer a clear, visual representation of the decision-making process.

- **Non-Linearity:** They can model complex, non-linear relationships without requiring linear separability.

Cons:

- **Overfitting Risk:** Decision Trees are prone to overfitting, particularly if they are too deep or not properly pruned.
- **Instability:** They can be unstable, as small changes in the data may lead to different tree structures.

It was obtained by using the Matlab function `fitctree(data, labels)` from the Statistics and Machine Learning Toolbox.

3.6.4 K-Nearest Neighbors (K-NN)

K-Nearest Neighbors (K-NN) is a straightforward, non-parametric method used for classification and regression. The classification of a new instance is determined by the majority vote of its k nearest neighbors in the feature space. The nearest neighbors are identified using distance metrics such as Euclidean, Manhattan, or Minkowski distance.

To classify a test instance \mathbf{x}_i , K-NN computes the distances to all training samples, selects the k closest ones, and assigns the class label based on the majority vote among these neighbors.

Pros:

- **Simplicity:** K-NN is easy to implement and does not require a training phase beyond storing the training data.
- **Adaptability:** It adapts well to local data structures and can model complex patterns effectively.

Cons:

- **Computational Cost:** The need to compute distances to all training examples makes K-NN computationally expensive for large datasets.
- **Feature Scaling Sensitivity:** K-NN's performance is sensitive to feature scaling, necessitating appropriate scaling of features.

It was obtained by using the Matlab function `fitcknn(data, labels, 'NumNeighbors', 5)` from the Statistics and Machine Learning Toolbox.

3.7 Methods of Evaluation

To assess the performance of the obtained classifiers, various machine learning metrics were employed. Their descriptions are based on [15], [11] and [17]. The following is a comprehensive list of the approaches utilized:

- **Loss:** It measures the model's average error across various evaluations, providing insight into its expected performance on new, unseen data. The loss value depends on the specific loss function used and can range from 0 to positive infinity, with lower values indicating better model performance.
- **Confusion Matrix:** It is a matrix, represented as a table, that outlines a classification model's performance by listing the counts of true positives (TP), true negatives (TN), false positives (FP), and false negatives (FN). This matrix aids in evaluating the model's effectiveness in classifying each class and highlights areas of misclassification.

$$\begin{matrix} TP & FP \\ FN & TN \end{matrix}$$

- **Precision:** It assesses the accuracy of the model in identifying positive predictions by calculating the proportion of true positives among all positive predictions made.

$$\text{Precision} = \frac{TP}{TP + FP}$$

Precision ranges from 0 to 1, where 1 indicates perfect precision (all positive predictions are true positives) and 0 indicates no true positives among the positive predictions.

- **Recall:** It measures the model's effectiveness in identifying all relevant positive instances, calculated as the ratio of true positives (TP) to the total number of actual positive cases

$$\text{Recall} = \frac{TP}{TP + FN}$$

Recall ranges from 0 to 1, with 1 indicating that all actual positives were correctly identified (perfect recall), and 0 indicating none of the actual positives were identified.

- **F1-Score:** It is the harmonic mean of Precision and Recall, combining these metrics into a single measure particularly useful for evaluating imbalanced datasets

$$F1\text{-Score} = 2 \cdot \frac{\text{Precision} \cdot \text{Recall}}{\text{Precision} + \text{Recall}}$$

It ranges from 0 to 1, where 1 indicates perfect Precision and Recall, and 0 represents the worst performance, where either Precision or Recall is zero.

- **Specificity:** it measures the proportion of true negatives out of all actual negatives, and indicates how effectively the model identifies negative instances.

$$\text{Specificity} = \frac{TN}{TN + FP}$$

Specificity ranges from 0 to 1. A specificity of 1 means perfect identification of negative instances (no false positives), while 0 means all negatives were incorrectly classified as positives.

- **Accuracy:** Accuracy represents the ratio of correctly predicted instances (both positive and negative) to the total number of instances.

$$\text{Accuracy} = \frac{TP + TN}{TP + TN + FP + FN}$$

It ranges from 0 to 1, where 1 signifies perfect classification of all instances, and 0 indicates complete misclassification.

- **False Positive Rate (FPR):** FPR measures the proportion of actual negatives that were incorrectly classified as positives.

$$FPR = \frac{FP}{FP + TN}$$

It ranges from 0 to 1, where 0 means no negative instances were misclassified as positives (perfect specificity), and 1 means all negatives were misclassified.

- **False Negative Rate (FNR):** it quantifies the proportion of actual positives that were mistakenly classified as negatives.

$$FNR = \frac{FN}{FN + TP}$$

It ranges from 0 to 1. A value of 0 indicates that all positive instances were correctly identified (perfect recall), while 1 means none of the positives were correctly identified.

- **Matthews Correlation Coefficient (MCC):** MCC provides a balanced measure of classification quality, taking into account all four categories of the confusion matrix.

$$MCC = \frac{TP \cdot TN - FP \cdot FN}{(TP + FP)(TP + FN)(TN + FP)(TN + FN)}$$

MCC ranges from -1 to 1. A value of 1 indicates perfect prediction, 0 means random predictions, and -1 indicates total disagreement between prediction and actual labels.

- **Balanced Accuracy:** it is the average of Recall for each class, providing a more reliable measure when classes are imbalanced.

$$\text{Balanced Accuracy} = \frac{1}{2} \frac{TP}{TP + FN} + \frac{TN}{TN + FP}$$

It ranges from 0 to 1, with 1 indicating perfect classification of both positive and negative classes, and 0 meaning all classes were misclassified.

- **Global Accuracy:** It calculates the proportion of accurate predictions relative to the total number of cases.
- **Cohen's Kappa:** It gauges how well two raters or models agree with each other, factoring in the probability of agreement happening by chance.

$$\text{Cohen's Kappa} = \frac{P_o - P_e}{1 - P_e}$$

with P_o representing the observed concordance, and P_e indicating the expected one by chance. Kappa ranges from -1 to 1, where 1 signifies perfect agreement, 0 indicates agreement no better than chance, and negative values imply worse-than-chance agreement.

3.8 Cross-Validation

In this thesis, the Leave-One-Out Cross-Validation (LOOCV) technique was employed to validate the models developed. The approach involved using 19 datasets to train the model and reserving one dataset for testing. This process was repeated over 20 iterations, with a different dataset serving as the test set in each iteration.

LOOCV is a specific case of k -fold cross-validation, where k equals the total number of observations in the dataset. In this approach, the model undergoes training n times, with n representing the number of data points. During each iteration, a single observation is excluded from the training data and designated as the test set, while the remaining $n - 1$ observations are used for training.

The procedure starts by selecting one data point to act as the validation set, with the model trained on the rest of the data. After predicting this particular data point, the resulting error is documented. This process is carried out for every data point in the dataset, ensuring each one is used as a validation set exactly once. The model's overall performance is then assessed by averaging the errors recorded across all iterations.

LOOCV offers the advantage of using nearly all available data for training in each iteration, which often results in a model that generalizes well. However, it can be computationally demanding, especially with large datasets, as it requires n training iterations. Additionally, the performance estimate's variance can be high because the training sets across iterations differ by only one data point. Nonetheless, LOOCV is particularly beneficial in scenarios involving small datasets, where every data point is crucial for model evaluation.

Chapter 4

Results

This chapter presents the results obtained using three distinct approaches: a non-standard-function-based (NSF-based) feature selection method and two standard-function-based (SF-based) methods. The SF-based methods are further divided into two categories: a tailored approach, where features are selected and optimized for each specific iteration of the leave-one-out cross-validation, and a one-size-fits-all approach, where the same set of features is used across all iterations.

To ensure clarity and brevity, the metrics will be presented for the average results obtained across the 20 iterations.

Since the datasets were created through data segmentation of the original signals, it is likely that the results will be more optimistic than they should be.

4.1 Results of the NSF-based method

The NSF-based feature selection was carried out using a combination of manually written functions that employed a traditional top-down approach aimed at the groups of features instead of the singular one. Once the groups of features were identified, the Matlab function 'relieff' was applied to select the most significant 75%.

The best results were obtained by taking into consideration the following groups of features related to the connectivity indicators: Standard deviation of the Phase Locking Value, Standard deviation of the Spectral Coherence, Standard deviation of the Phase Slope Index, Standard deviation of the Partial Directed Coherence, Skewness of the Directed Transfer Function, Standard deviation of the Mutual In-

formation, Indices of Granger Causality, Skewness of the Coherence in Amplitude, Skewness of the Phase Locking Value, Kurtosis of the Phase Locking Value, Kurtosis of the Phase Lag Index, Skewness of the Partial Directed Coherence, Kurtosis of the Directed Transfer Function.

The features correlated to non-connectivity indicators, that were used are: Standard deviation of the Root Mean Square, and Relative Power of Rhythms.

Ranking the four classifiers from best to worst, we have: k-NN, Decision Tree, Fisher, and SVM. The k-NN classifier outperforms the others significantly, while Fisher and Decision Tree yield similar results. The SVM classifier, however, performs the worst by a considerable margin.

4.1.1 NSF-B - Fisher

Table 4.1: Confusion Matrix of the NSF-based Fisher's model

| | Prediction GOS 1 | Prediction GOS 3 | Prediction GOS 5 |
|--------------|-------------------------|-------------------------|-------------------------|
| GOS 1 | 46 | 5 | 5 |
| GOS 3 | 10 | 57 | 4 |
| GOS 5 | 3 | 1 | 86 |

Table 4.2: Machine learning metrics of the NSF-based Fisher's model

| | GOS 1 | GOS 3 | GOS 5 |
|--------------------------|--------------|--------------|--------------|
| Precision | 0.7797 | 0.9048 | 0.9053 |
| Recall | 0.8214 | 0.8028 | 0.9556 |
| F1 Score | 0.8000 | 0.8507 | 0.9297 |
| Specificity | 0.9193 | 0.9589 | 0.9291 |
| Accuracy | 0.8940 | 0.9078 | 0.9401 |
| FPR | 0.0807 | 0.0411 | 0.0709 |
| FNR | 0.1786 | 0.1972 | 0.0444 |
| MCC | 0.7284 | 0.7874 | 0.8786 |
| Balanced Accuracy | 0.8703 | 0.8809 | 0.9423 |

Table 4.3: Machine learning global metrics of the NSF-based Fisher's model

| | Loss | Global Accuracy | Cohen Kappa |
|--------------|-------------|------------------------|--------------------|
| Value | 0.1290 | 0.8710 | 0.8088 |

4.1.2 NSF-B - Support Vector Machine

Table 4.4: Confusion Matrix of the NSF-based SVM's model

| | Prediction GOS 1 | Prediction GOS 3 | Prediction GOS 5 |
|--------------|-------------------------|-------------------------|-------------------------|
| GOS 1 | 23 | 25 | 8 |
| GOS 3 | 13 | 47 | 11 |
| GOS 5 | 1 | 2 | 87 |

Table 4.5: Machine learning metrics of the NSF-based SVM's model

| | GOS 1 | GOS 3 | GOS 5 |
|--------------------------|--------------|--------------|--------------|
| Precision | 0.6216 | 0.6351 | 0.8208 |
| Recall | 0.4107 | 0.6620 | 0.9667 |
| F1 Score | 0.4946 | 0.6483 | 0.8878 |
| Specificity | 0.9130 | 0.8151 | 0.8504 |
| Accuracy | 0.7834 | 0.7650 | 0.8986 |
| FPR | 0.0870 | 0.1849 | 0.1496 |
| FNR | 0.5893 | 0.3380 | 0.0333 |
| MCC | 0.3767 | 0.4721 | 0.8053 |
| Balanced Accuracy | 0.6619 | 0.7385 | 0.9085 |

Table 4.6: Machine learning global metrics of the NSF-based SVM's model

| | Loss | Global Accuracy | Cohen Kappa |
|--------------|-------------|------------------------|--------------------|
| Value | 0.2765 | 0.7235 | 0.6004 |

4.1.3 NSF-B - Decision Tree

Table 4.7: Confusion Matrix of the NSF-based Decision Tree's model

| | Prediction GOS 1 | Prediction GOS 3 | Prediction GOS 5 |
|--------------|-------------------------|-------------------------|-------------------------|
| GOS 1 | 48 | 5 | 3 |
| GOS 3 | 5 | 59 | 7 |
| GOS 5 | 2 | 8 | 80 |

Table 4.8: Machine learning metrics of the NSF-based Decision Tree's model

| | Class 1 | Class 2 | Class 3 |
|--------------------------|----------------|----------------|----------------|
| Precision | 0.8727 | 0.8194 | 0.8889 |
| Recall | 0.8571 | 0.8310 | 0.8889 |
| F1 Score | 0.8649 | 0.8252 | 0.8889 |
| Specificity | 0.9565 | 0.9110 | 0.9213 |
| Accuracy | 0.9309 | 0.8848 | 0.9078 |
| FPR | 0.0435 | 0.0890 | 0.0787 |
| FNR | 0.1429 | 0.1690 | 0.1111 |
| MCC | 0.8185 | 0.7393 | 0.8101 |
| Balanced Accuracy | 0.9068 | 0.8710 | 0.9051 |

Table 4.9: Machine learning global metrics of the NSF-based Decision Tree's model

| | Loss | Global Accuracy | Cohen Kappa |
|--------------|-------------|------------------------|--------------------|
| Value | 0.1382 | 0.8618 | 0.7946 |

4.1.4 NSF-B - k-Nearest Neighbors

Table 4.10: Confusion Matrix of the NSF-based K-NN's model

| | Prediction GOS 1 | Prediction GOS 3 | Prediction GOS 5 |
|--------------|-------------------------|-------------------------|-------------------------|
| GOS 1 | 47 | 4 | 5 |
| GOS 3 | 0 | 68 | 3 |
| GOS 5 | 3 | 2 | 85 |

Table 4.11: Machine learning metrics of the NSF-based K-NN's model

| | GOS 1 | GOS 3 | GOS 5 |
|--------------------------|--------------|--------------|--------------|
| Precision | 0.9400 | 0.9189 | 0.9140 |
| Recall | 0.8393 | 0.9577 | 0.9444 |
| F1 Score | 0.8868 | 0.9379 | 0.9290 |
| Specificity | 0.9814 | 0.9589 | 0.9370 |
| Accuracy | 0.9447 | 0.9585 | 0.9401 |
| FPR | 0.0186 | 0.0411 | 0.0630 |
| FNR | 0.1607 | 0.0423 | 0.0556 |
| MCC | 0.8528 | 0.9072 | 0.8775 |
| Balanced Accuracy | 0.9103 | 0.9583 | 0.9407 |

Table 4.12: Machine learning global metrics of the NSF-based Decision Tree's model

| | Loss | Global Accuracy | Cohen Kappa |
|--------------|-------------|------------------------|--------------------|
| Value | 0.0783 | 0.9217 | 0.8842 |

4.2 Results of the SF-based one-size method

This approach used feature selection functions, such as ReliefF, to refine the dataset. Starting with all 54 available feature groups, 7 were selected. These selected features were then used to construct the feature matrices for each evaluation's training and testing sets. Of these 8 groups, 4 were of connectivity features and 3 of non-connectivity.

The groups of connectivity features were:

Standard Deviation of the Directed Transfer Function, Skewness of the Partial Directed Coherence, Standard Deviation of the Phase Slope Index, Kurtosis of the Spectral Coherence.

While the groups of non-connectivity features were:

Skewness of the Entropy, Skewness of the Frequency Median, Kurtosis of the Hurst Exponent.

Ranking the four classifiers from best to worst, we have: k-NN, Fisher, Decision Tree, and SVM. The k-NN classifier outperforms the others significantly, while Fisher and Decision Tree yield similar results. The SVM classifier, however, performs the worst by a considerable margin.

4.2.1 SF-B-OS - Fisher

Table 4.13: Confusion Matrix of the SF-based one-size method Fisher model

| | Prediction GOS 1 | Prediction GOS 3 | Prediction GOS 5 |
|--------------|-------------------------|-------------------------|-------------------------|
| GOS 1 | 46 | 5 | 5 |
| GOS 3 | 10 | 57 | 4 |
| GOS 5 | 3 | 1 | 86 |

Table 4.14: Machine learning metrics of the SF-based one-size method Fisher model

| | GOS 1 | GOS 3 | GOS 5 |
|--------------------------|--------------|--------------|--------------|
| Precision | 0.7797 | 0.9048 | 0.9053 |
| Recall | 0.8214 | 0.8028 | 0.9556 |
| F1 Score | 0.8000 | 0.8507 | 0.9297 |
| Specificity | 0.9193 | 0.9589 | 0.9291 |
| Accuracy | 0.8940 | 0.9078 | 0.9401 |
| FPR | 0.0807 | 0.0411 | 0.0709 |
| FNR | 0.1786 | 0.1972 | 0.0444 |
| MCC | 0.7284 | 0.7874 | 0.8786 |
| Balanced Accuracy | 0.8703 | 0.8809 | 0.9423 |

Table 4.15: Machine learning global metrics of the SF-based one-size method Fisher model

| | Loss | Global Accuracy | Cohen Kappa |
|--------------|-------------|------------------------|--------------------|
| Value | 0.1290 | 0.8710 | 0.8088 |

4.2.2 SF-B-OS - Support Vector Machine

Table 4.16: Confusion Matrix of the SF-based one-size method SVM model

| | Prediction GOS 1 | Prediction GOS 3 | Prediction GOS 5 |
|--------------|-------------------------|-------------------------|-------------------------|
| GOS 1 | 23 | 25 | 8 |
| GOS 3 | 13 | 47 | 11 |
| GOS 5 | 1 | 2 | 87 |

Table 4.17: Machine learning metrics of the SF-based one-size method SVM model

| | GOS 1 | GOS 3 | GOS 5 |
|--------------------------|--------------|--------------|--------------|
| Precision | 0.6216 | 0.6351 | 0.8208 |
| Recall | 0.4107 | 0.6620 | 0.9667 |
| F1 Score | 0.4946 | 0.6483 | 0.8878 |
| Specificity | 0.9130 | 0.8151 | 0.8504 |
| Accuracy | 0.7834 | 0.7650 | 0.8986 |
| FPR | 0.0870 | 0.1850 | 0.1496 |
| FNR | 0.5893 | 0.3380 | 0.0333 |
| MCC | 0.3767 | 0.4721 | 0.8053 |
| Balanced Accuracy | 0.6619 | 0.7385 | 0.9085 |

Table 4.18: Machine learning global metrics of the SF-based one-size method SVM model

| | Loss | Global Accuracy | Cohen Kappa |
|--------------|-------------|------------------------|--------------------|
| Value | 0.2765 | 0.7235 | 0.6004 |

4.2.3 SF-B-OS - Decision Tree

Table 4.19: Confusion Matrix of the SF-based one-size method Decision Tree model

| | Prediction GOS 1 | Prediction GOS 3 | Prediction GOS 5 |
|--------------|-------------------------|-------------------------|-------------------------|
| GOS 1 | 48 | 5 | 3 |
| GOS 3 | 5 | 59 | 7 |
| GOS 5 | 2 | 8 | 80 |

Table 4.20: Machine learning metrics of the SF-based one-size method Decision Tree model

| | GOS 1 | GOS 3 | GOS 5 |
|--------------------------|--------------|--------------|--------------|
| Precision | 0.8727 | 0.8194 | 0.8889 |
| Recall | 0.8571 | 0.8310 | 0.8889 |
| F1 Score | 0.8649 | 0.8252 | 0.8889 |
| Specificity | 0.9565 | 0.9110 | 0.9213 |
| Accuracy | 0.9309 | 0.8848 | 0.9078 |
| FPR | 0.0435 | 0.0890 | 0.0787 |
| FNR | 0.1429 | 0.1690 | 0.1111 |
| MCC | 0.8185 | 0.7393 | 0.8101 |
| Balanced Accuracy | 0.9068 | 0.8710 | 0.9051 |

Table 4.21: Machine learning global metrics of the SF-based one-size method Decision Tree model

| | Loss | Global Accuracy | Cohen Kappa |
|--------------|-------------|------------------------|--------------------|
| Value | 0.1382 | 0.8618 | 0.7946 |

4.2.4 SF-B-OS - k Nearest Neighbors

Table 4.22: Confusion Matrix of the SF-based one-size method K-NN's model

| | Prediction GOS 1 | Prediction GOS 3 | Prediction GOS 5 |
|--------------|-------------------------|-------------------------|-------------------------|
| GOS 1 | 47 | 4 | 5 |
| GOS 3 | 0 | 68 | 3 |
| GOS 5 | 3 | 2 | 85 |

Table 4.23: Machine learning metrics of the SF-based one-size method K-NN's model

| | GOS 1 | GOS 3 | GOS 5 |
|--------------------------|--------------|--------------|--------------|
| Precision | 0.9400 | 0.9189 | 0.9140 |
| Recall | 0.8393 | 0.9577 | 0.9444 |
| F1 Score | 0.8868 | 0.9379 | 0.9290 |
| Specificity | 0.9814 | 0.9589 | 0.9370 |
| Accuracy | 0.9447 | 0.9585 | 0.9401 |
| FPR | 0.0186 | 0.0411 | 0.0630 |
| FNR | 0.1607 | 0.0423 | 0.0556 |
| MCC | 0.8528 | 0.9072 | 0.8775 |
| Balanced Accuracy | 0.9103 | 0.9583 | 0.9407 |

Table 4.24: Machine learning global metrics of the SF-based one-size method k-NN model

| | Loss | Global Accuracy | Cohen Kappa |
|--------------|-------------|------------------------|--------------------|
| Value | 0.0783 | 0.9217 | 0.8842 |

4.3 Results of the SF-based tailored method

This approach employed feature selection functions, such as 'relieff', to refine the dataset. Beginning with all 54 available feature groups, a varying number of these groups were selected for each evaluation, based on which configuration provided the best results for each specific test. The chosen features were then used to construct the feature matrices for the corresponding training and testing sets of each evaluation. 16 feature groups appeared in 90% of the evaluations, and, of these 16, 13 were of connectivity and 3 of non-connectivity.

The groups of connectivity features were:

Directed Transfer Function Kurtosis, Directed Transfer Function Skewness, Granger Causality, Mutual Information Standard Deviation, Partial Directed Coherence Skewness, Partial Directed Coherence Standard Deviation, Phase Lag Index Standard Deviation, Amplitude Coherence Kurtosis, Amplitude Coherence Skewness, Spectral Coherence Kurtosis, Spectral Coherence Skewness, Spectral Coherence Standard Deviation.

The groups of non-connectivity features were:

Entropy Standard Deviation, Root Mean Square Standard Deviation, Relative Power of the Rhythms.

Ranking the four classifiers from best to worst in terms of performance, we have k-NN and Fisher tied for first place, followed by SVM, and then Decision Tree.

Although Fisher and k-NN classifiers perform equally well overall, Fisher is less accurate in classifying GOS1, whereas k-NN struggles more with GOS3.

The Decision Tree's results are significantly poorer, with more than twice the number of misclassifications compared to SVM, which itself has three times the misclassifications of the top two classifiers.

4.3.1 SF-B-T - Fisher

Table 4.25: Confusion Matrix of the SF-based tailored method Fisher model

| | Prediction GOS 1 | Prediction GOS 3 | Prediction GOS 5 |
|--------------|-------------------------|-------------------------|-------------------------|
| GOS 1 | 54 | 2 | 0 |
| GOS 3 | 0 | 71 | 0 |
| GOS 5 | 1 | 0 | 89 |

Table 4.26: Machine learning metrics of the SF-based tailored method Fisher model

| | GOS 1 | GOS 3 | GOS 5 |
|--------------------------|--------------|--------------|--------------|
| Precision | 0.9818 | 0.9726 | 1.0000 |
| Recall | 0.9643 | 1.0000 | 0.9889 |
| F1 Score | 0.9730 | 0.9861 | 0.9944 |
| Specificity | 0.9938 | 0.9863 | 1.0000 |
| Accuracy | 0.9862 | 0.9908 | 0.9954 |
| FPR | 0.0062 | 0.0137 | 0.0000 |
| FNR | 0.0357 | 0.0000 | 0.0111 |
| MCC | 0.9638 | 0.9794 | 0.9905 |
| Balanced Accuracy | 0.9790 | 0.9932 | 0.9944 |

Table 4.27: Machine learning global metrics of the SF-based tailored method Fisher model

| | Loss | Global Accuracy | Cohen Kappa |
|--------------|-------------|------------------------|--------------------|
| Value | 0.0138 | 0.9862 | 0.9795 |

4.3.2 SF-B-T - Support Vector Machine

Table 4.28: Confusion Matrix of the SF-based tailored method SVM model

| | Prediction GOS 1 | Prediction GOS 3 | Prediction GOS 5 |
|--------------|-------------------------|-------------------------|-------------------------|
| GOS 1 | 53 | 1 | 2 |
| GOS 3 | 2 | 65 | 4 |
| GOS 5 | 0 | 1 | 89 |

Table 4.29: Machine learning metrics of the SF-based tailored method SVM model

| | GOS 1 | GOS 3 | GOS 5 |
|--------------------------|--------------|--------------|--------------|
| Precision | 0.9636 | 0.9701 | 0.9368 |
| Recall | 0.9464 | 0.9155 | 0.9889 |
| F1 Score | 0.9550 | 0.9420 | 0.9622 |
| Specificity | 0.9876 | 0.9863 | 0.9528 |
| Accuracy | 0.9769 | 0.9631 | 0.9677 |
| FPR | 0.0124 | 0.0137 | 0.0472 |
| FNR | 0.0536 | 0.0845 | 0.0111 |
| MCC | 0.9395 | 0.9159 | 0.9351 |
| Balanced Accuracy | 0.9670 | 0.9509 | 0.9708 |

Table 4.30: Machine learning global metrics of the SF-based tailored method SVM model

| | Loss | Global Accuracy | Cohen Kappa |
|--------------|-------------|------------------------|--------------------|
| Value | 0.0461 | 0.9539 | 0.9318 |

4.3.3 SF-B-T - Decision Tree

Table 4.31: Confusion Matrix of the SF-based tailored method Decision Tree model

| | Prediction GOS 1 | Prediction GOS 3 | Prediction GOS 5 |
|--------------|-------------------------|-------------------------|-------------------------|
| GOS 1 | 51 | 2 | 3 |
| GOS 3 | 1 | 63 | 7 |
| GOS 5 | 5 | 7 | 78 |

Table 4.32: Machine learning metrics of the SF-based tailored method Decision Tree model

| | GOS 1 | GOS 3 | GOS 5 |
|--------------------------|--------------|--------------|--------------|
| Precision | 0.8947 | 0.8750 | 0.8864 |
| Recall | 0.9107 | 0.8873 | 0.8667 |
| F1 Score | 0.9027 | 0.8811 | 0.8764 |
| Specificity | 0.9627 | 0.9384 | 0.9213 |
| Accuracy | 0.9493 | 0.9217 | 0.8986 |
| FPR | 0.0373 | 0.0616 | 0.0787 |
| FNR | 0.0893 | 0.1127 | 0.1333 |
| MCC | 0.8685 | 0.8227 | 0.7906 |
| Balanced Accuracy | 0.9367 | 0.9128 | 0.8940 |

Table 4.33: Machine learning global metrics of the SF-based tailored method Decision Tree model

| | Loss | Global Accuracy | Cohen Kappa |
|--------------|-------------|------------------------|--------------------|
| Value | 0.1152 | 0.8848 | 0.8285 |

4.3.4 SF-B-T - k Nearest Neighbors

Table 4.34: Confusion Matrix of the SF-based tailored method K-NN's model

| | Prediction GOS 1 | Prediction GOS 3 | Prediction GOS 5 |
|--------------|-------------------------|-------------------------|-------------------------|
| GOS 1 | 55 | 1 | 0 |
| GOS 3 | 0 | 71 | 0 |
| GOS 5 | 1 | 1 | 88 |

Table 4.35: Machine learning metrics of the SF-based tailored method K-NN's model

| | GOS 1 | GOS 3 | GOS 5 |
|--------------------------|--------------|--------------|--------------|
| Precision | 0.9821 | 0.9726 | 1.0000 |
| Recall | 0.9821 | 1.0000 | 0.9778 |
| F1 Score | 0.9821 | 0.9861 | 0.9888 |
| Specificity | 0.9938 | 0.9863 | 1.0000 |
| Accuracy | 0.9908 | 0.9908 | 0.9908 |
| FPR | 0.0062 | 0.0137 | 0.0000 |
| FNR | 0.0179 | 0.0000 | 0.0222 |
| MCC | 0.9759 | 0.9794 | 0.9811 |
| Balanced Accuracy | 0.98797 | 0.99315 | 0.98889 |

Table 4.36: Machine learning global metrics of the SF-based tailored method K-NN model

| | Loss | Global Accuracy | Cohen Kappa |
|--------------|-------------|------------------------|--------------------|
| Value | 0.0138 | 0.9862 | 0.9794 |

4.4 Considerations

By observing the results of the three applied methods, the best results are given by the SF-based tailored method, while the NSF-based method and the SF-based one-size method gave the same overall performance.

In every method, the classifier that gave the best results was the k-NN, with Fisher second, Decision Tree third, and SVM last.

Based on these results, it can be inferred that the best performances are achieved by classifiers employing a geometric approach.

The connectivity indicators that were selected by multiple methods are:

- Skewness of the Partial Directed Coherence, which was selected in all three methods;
- Standard deviation of the Spectral Coherence, Standard deviation of the Mutual Information, Indices of Granger Causality, and Kurtosis of the Directed Transfer Function, which were selected in the NSF-based and SF-based tailored method;
- Kurtosis of the Spectral Coherence, which was selected in the two SF-based methods.

The non-connectivity indicators that were selected by multiple methods are:

- Standard deviation of the Root Mean Square, and Relative Power of the Rhythms, which were selected in the NSF-based and SF-based tailored method.

The selected connectivity indicators suggest that the directionality, causality, and complexity of interactions between brain regions are critical for predicting outcomes in coma patients, underscoring the importance of examining inter-regional brain communication in coma studies.

Chapter 5

Conclusion

This thesis has examined the predictive capabilities of both connectivity and non-connectivity indicators, with a primary focus on the former, in determining the likelihood of recovery in coma patients. By classifying electroencephalography (EEG) signals into specific Glasgow Outcome Scale (GOS) categories, the study has shed light on the importance of brain connectivity in evaluating patient prognosis.

The analysis demonstrated that certain indicators significantly contribute to the accurate classification of patients' recovery states. The application of machine learning models to these indicators showed promising results, indicating that it is possible to differentiate between various levels of consciousness and recovery outcomes. However, this study was limited by the small sample size and the number of EEG channels used, which may have impacted the robustness of the signal pre-processing and the reliability of the classification results.

Given these constraints, the findings should be interpreted with caution. The small number of patients, in particular, limits the generalizability of the results. To strengthen the conclusions drawn in this thesis, future research should aim to include a larger and more diverse patient population, with more extensive EEG recordings. This would allow for a more comprehensive analysis of the connectivity patterns and their relationship with recovery outcomes.

Moreover, the promising results of this study highlight the potential of brain connectivity, particularly the directionality and causality between different regions, as a biomarker for predicting coma outcomes. Future research should explore advanced machine learning techniques and more sophisticated connectivity measures to improve predictive accuracy.

References

In this section, the various chapters and sections will be associated with the material from which they were inspired.

1.1.1 [19]
1.1.2 [19]
1.1.3 [19]
1.1.4 [19]
1.2.1 [6] [33]
1.2.2 [6] [2]
1.2.3 [33]
1.3.1 [19]
1.3.2 [1]
1.3.3 [14] [24] [29]

2.1 [35]
2.2 [20] [3]

2.3 and 2.4 don't use a specific number of sources but were synthesized by reading several papers.

2.5.1 [22]
2.5.2 [34]
2.5.3 [18]
2.5.4 [28]
2.5.5 [10]
2.5.6 [32]
2.5.7 [36]

3.3 [5] [12] [27] [8]
3.4 [21] [30] [16] [9]
3.6 [15] [4]
3.7 [15] [11] [17]
3.8 [7]

Bibliography

- [1] ACRM AAN and NIDILRR. Summary of evidence-based guideline for families and caregivers disorders of consciousness. 2018.
- [2] Jayant N. Acharya, Abeer Hani, Janna Cheek, Partha Thirumala, and Tammy N. Tsuchida. Guideline 2: Guidelines for standard electrode position nomenclature. *American Clinical Neurophysiology Society*, 2021.
- [3] Kaveh Ajam, Laurie S. Gold, Stefanie S. Beck, Steve Damon, Robert Phelps, and Thomas D. Rea. Reliability of the cerebral performance category to classify neurological status among survivors of ventricular fibrillation arrest: a cohort study. *Scand J Trauma Resusc Emerg Med*, 19:38, Jun 15 2011.
- [4] Christopher M. Bishop. *Pattern Recognition and Machine Learning*. Springer, 2006.
- [5] Boualem Boashash. *Time-Frequency Analysis: Theory and Applications*. Elsevier, Amsterdam, 1992.
- [6] Jeffrey W Britton, Lauren C Frey, Jennifer L Hopp, Pearce Korb, Mohamad Z Koubeissi, William E Lievens, Elia M Pestana-Knight, and Erk K St Louis. Electroencephalography (eeg): An introductory text and atlas of normal and abnormal findings in adults, children, and infants. 2019.
- [7] Jason Brown. Loocv for evaluating machine learning algorithms. *Machine Learning Mastery*, 2020.
- [8] Eugene N Bruce. *Biomedical Signal Processing and Signal Modeling*. John Wiley & Sons, 2001.
- [9] C3.ai. Root mean square error (rmse), n.d. Specifically covers root mean square error (RMSE).
- [10] Srivas Chennu, Jitka Annen, Sarah Wannez, Aurore Thibaut, Camille Chatelle, Helena Cassol, Géraldine Martens, Caroline Schnakers, Olivia

Gosseries, David K. Menon, and Steven Laureys. Brain networks predict metabolism, diagnosis and prognosis at the bedside in disorders of consciousness. *Brain*, 2017.

- [11] Davide Chicco and Giuseppe Jurman. The advantages of the matthews correlation coefficient (mcc) over f1 score and accuracy in binary classification evaluation. *BMC Genomics*, 21(1):6, 2020. Available online: <https://bmcbioinformatics.biomedcentral.com/articles/10.1186/s12859-019-3431-6>.
- [12] Thomas M Cover and Joy A Thomas. *Elements of Information Theory*. John Wiley & Sons, 2006.
- [13] M. I. Garrido, J. M. Kilner, K. E. Stephan, and K. J. Friston. The mismatch negativity: a review of underlying mechanisms. *Clin Neurophysiol*, 120(3):453–463, Mar 2009. Epub 2009 Jan 31.
- [14] Ajay Kumar Goila and Mridula Pawar. The diagnosis of brain death. *Indian Journal of Critical Care Medicine: peer-reviewed, official publication of Indian Society of Critical Care Medicine*, 13(1):7, 2009.
- [15] Trevor Hastie, Robert Tibshirani, and Jerome Friedman. *The Elements of Statistical Learning: Data Mining, Inference, and Prediction*. Springer, 2009. Available online: <https://web.stanford.edu/~hastie/ElemStatLearn/>.
- [16] Investopedia. Statistical measures, n.d. Provides definitions and explanations for standard deviation, variance, skewness, kurtosis, probability density functions (PDF), and root mean square error (RMSE).
- [17] Gareth James, Daniela Witten, Trevor Hastie, and Robert Tibshirani. *Introduction to Statistical Learning: with Applications in R*. Springer, 2013. Available online: <https://www.statlearning.com/>.
- [18] Mengdi Jiang, Yingying Su, Gang Liu, Huijin Huang, and Fei Tian. Eeg pattern predicts awakening of comatose patients after cardiopulmonary resuscitation. *Resuscitation*, 2020.
- [19] Eric R Kandel, James H Schwartz, Thomas M Jessell, Steven Siegelbaum, A James Hudspeth, Sarah Mack, et al. *Principles of neural science*. McGraw-hill New York, 5th edition, 2013.
- [20] Joshua Kornbluth and Anup Bhardwaj. Evaluation of coma: a critical appraisal of popular scoring systems. *Neurocrit Care*, 14(1):134–143, Feb 2011.

- [21] William Mendenhall, Robert J. Beaver, and Barbara M. Beaver. *Introduction to Probability and Statistics*. Cengage Learning, Boston, 13th edition, 2013.
- [22] J.A.M. Michel, Jeannette van Putten, Barry J. Hofmeijer, Marleen C. Ruitter, and Tjepkema-Cloostermans. Deep learning for outcome prediction of postanoxic coma. *Journal Name*, 2017.
- [23] I. F. Neves, I. C. Gonçalves, R. A. Leite, F. C. Magliaro, and C. G. Matas. Middle latency response study of auditory evoked potentials amplitudes and latencies in audio-logically normal individuals. *Braz J Otorhinolaryngol*, 73(1):69–74, Jan-Feb 2007.
- [24] NHS. Brain death, 2023. Accessed: 27 October 2023.
- [25] Christos P Panteliadis. Historical overview of electroencephalography: from antiquity to the beginning of the 21st century. *J. Brain Neurol. Disord*, 3:1–10, 2021.
- [26] T. W. Picton. The P300 wave of the human event-related potential. *J Clin Neurophysiol*, 9(4):456–479, Oct 1992.
- [27] Steven M Pincus. Approximate entropy as a measure of system complexity. *Proceedings of the National Academy of Sciences*, 88(6):2297–2301, 1991.
- [28] M. Spallitti, Riccardo Carrai, Maenia Scarpino, C. Cossu, A. Ammannati, M. Ciapetti, L. Tadini Buoninsegni, Adriano Peris, Serafina Valente, Antonello Grippo, and Aldo Amantini. Single electroencephalographic patterns as specific and time-dependent indicators of good and poor outcome after cardiac arrest. *Clinical Neurophysiology*, 2016.
- [29] William Spears, Asim Mian, and David Greer. Brain death: a clinical overview. *Journal of Intensive Care*, 10(1):1–16, 2022.
- [30] StatTrek. Statistics tutorials, n.d. Covers standard deviation, variance, skewness, kurtosis, probability density functions (PDF), and root mean square error (RMSE).
- [31] Sydney North Neurology and Neurophysiology. Brainstem auditory evoked potential (baep), 2021.
- [32] Tao Tao, Nan Hu, Chenyang Xu, Fajun Li, Qin Wang, and Yuan Peng. Prognosis of comatose patients with reduced eeg montage by combining quantitative eeg features in various domains. *Frontiers in Neuroscience*, 2023.

- [33] Michal Teplan et al. Fundamentals of eeg measurement. *Measurement science review*, 2(2):1–11, 2002.
- [34] Athina Tzovara, Micah Murray, Gijs Plomp, Michael H. Herzog, Christoph M. Michel, and Marzia De Lucia. Decoding stimulus-related information from single-trial eeg responses based on voltage topographies. *Pattern Recognition*, 2012.
- [35] J. T. J. M. van Dijck, C. Q. B. Mostert, A. P. A. Greeven, E. J. O. Kompanje, W. C. Peul, G. C. W. de Ruiter, and S. Polinder. Functional outcome, in-hospital healthcare consumption and in-hospital costs for hospitalised traumatic brain injury patients: a dutch prospective multicentre study. *Acta Neurochir (Wien)*, 162(7):1607–1618, Jul 2020. Epub 2020 May 14.
- [36] Yuzhang Wu, Zhitao Li, Ruowei Qu, Yangang Wang, Zhongzhen Li, Le Wang, Keke Feng, Yifeng Cheng, and Shaoya Yin. Electroencephalogram-based brain connectivity analysis in prolonged disorders of consciousness. *Neural Plasticity*, pages 1–18, 2023.